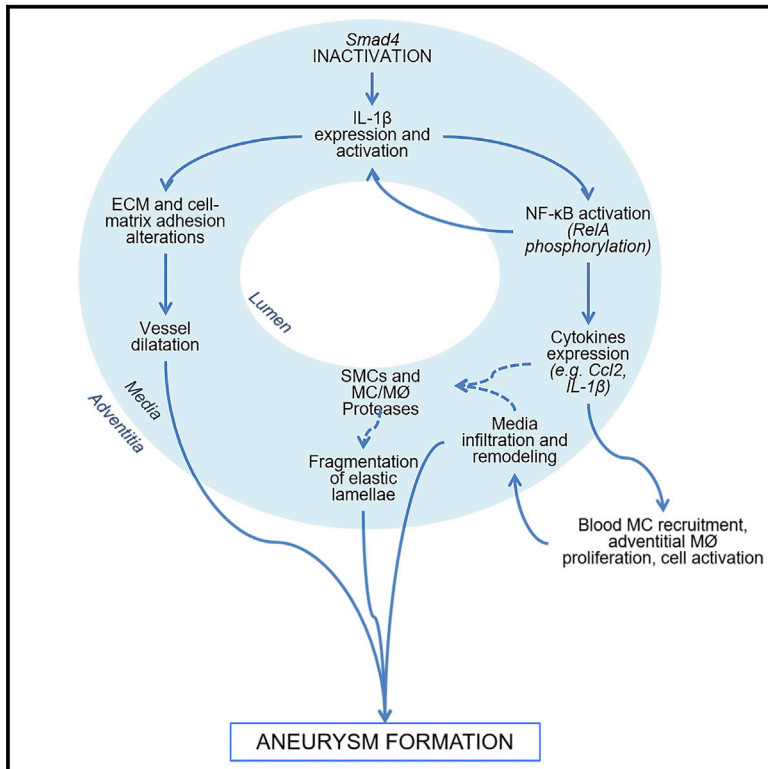


Immunity

Targeting Interleukin-1 β Protects from Aortic Aneurysms Induced by Disrupted Transforming Growth Factor β Signaling

Graphical Abstract



Authors

Francesco Da Ros,
Raimondo Carnevale,
Giuseppe Cifelli, ..., Paola Braghetta,
Giuseppe Lembo, Daniela Carnevale

Correspondence

braggett@bio.unipd.it (P.B.),
lembo@neuromed.it (G.L.),
daniela.carnevale@neuromed.it (D.C.)

In Brief

TGF- β signaling has an unquestionable but still controversial role in the pathogenesis of aortic aneurysm. Da Ros et al. demonstrate that disruption of TGF- β signaling in SMCs activates an autocrine IL-1 β pathway that acts as a danger signal to recruit innate immune cells in the adventitia through CCL2.

Highlights

- SMC-specific inducible deletion of *Smad4* in adult mice provokes aortic aneurysms
- The resulting disrupted TGF- β signaling activates IL-1 β in SMCs as a danger signal
- IL-1 β induces CCL2 to recruit an innate immune response harmful to the aortic walls
- Targeting IL-1 β and CCL2 protects mice with disrupted TGF- β in SMCs from aneurysms



Targeting Interleukin-1 β Protects from Aortic Aneurysms Induced by Disrupted Transforming Growth Factor β Signaling

Francesco Da Ros,^{1,2} Raimondo Carnevale,³ Giuseppe Cifelli,³ Dario Bizzotto,¹ Manuel Casaburo,³ Marialuisa Perrotta,³ Lorenzo Carnevale,³ Iolanda Vinciguerra,³ Stefania Fardella,³ Roberta Iacobucci,³ Giorgio M. Bressan,¹ Paola Braghetta,^{1,*} Giuseppe Lembo,^{2,3,4,*} and Daniela Carnevale^{2,3,*}

¹Department of Molecular Medicine, University of Padova, Padua 35131, Italy

²Department of Molecular Medicine, "Sapienza" University of Rome, 00161 Rome, Italy

³Department of Angiocardioneurology and Translational Medicine, IRCCS Neuromed, 86077 Pozzilli, Italy

⁴Lead Contact

*Correspondence: braghetta@bio.unipd.it (P.B.), lembo@neuromed.it (G.L.), daniela.carnevale@neuromed.it (D.C.)

<https://doi.org/10.1016/j.immuni.2017.10.016>

SUMMARY

Aortic aneurysms are life-threatening conditions with effective treatments mainly limited to emergency surgery or trans-arterial endovascular stent grafts, thus calling for the identification of specific molecular targets. Genetic studies have highlighted controversial roles of transforming growth factor β (TGF- β) signaling in aneurysm development. Here, we report on aneurysms developing in adult mice after smooth muscle cell (SMC)-specific inactivation of *Smad4*, an intracellular transducer of TGF- β . The results revealed that *Smad4* inhibition activated interleukin-1 β (IL-1 β) in SMCs. This danger signal later recruited innate immunity in the adventitia through chemokine (C-C motif) ligand 2 (CCL2) and modified the mechanical properties of the aortic wall, thus favoring vessel dilation. SMC-specific *Smad4* deletion in *Il1r1*- or *Ccr2*-null mice resulted in milder aortic pathology. A chronic treatment with anti-IL-1 β antibody effectively hampered aneurysm development. These findings identify a mechanistic target for controlling the progression of aneurysms with compromised TGF- β signaling, such as those driven by *SMAD4* mutations.

INTRODUCTION

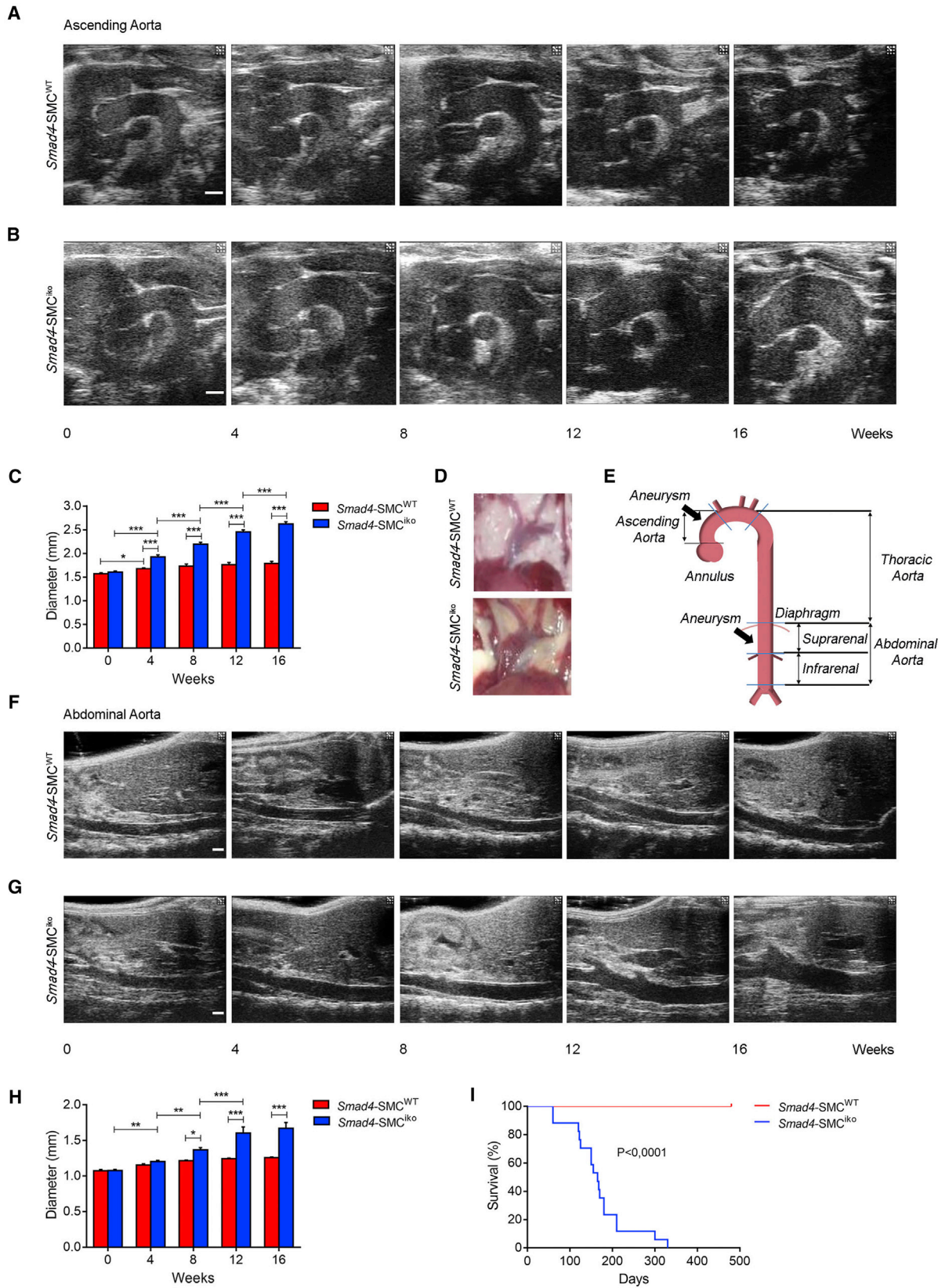
Defined as a progressive dilation of the vessel, with tube-shaped (fusiform) or round (saccular) enlargements, aortic aneurysms are a significant cause of mortality and morbidity in the western world; they have no clinical treatment other than high-risk surgery or trans-arterial endovascular therapies with stent grafts when the conditions of patients are favorable to this option (Davis et al., 2014; Milewicz et al., 2008). However, the indication for intervention is generally reserved for large aneurysms, and no effective therapy contrasts the evolution of aneurysms at initial stages. This shortage of clinical approaches is mainly a result

of insufficient insights into the early pathogenetic mechanisms of aneurysm formation. Among the proposed signals involved, components of the transforming growth factor β (TGF- β) pathway have an unquestionable but still controversial role in the pathogenesis of aortic aneurysms (Gillis et al., 2013; Lindsay and Dietz, 2011).

When mutated, genes encoding components of the TGF- β pathway can cause the formation of aortic aneurysms, leading to, for instance, Loeys-Dietz syndrome (LDS) (Gillis et al., 2013). The observation that aortic tissue from LDS patients has defective TGF- β signaling components but paradoxically enhanced TGF- β activity, as shown by increased phosphorylation of its downstream intracellular signaling SMAD2, led to the proposal that TGF- β hyperactivity accounts for the aortic pathology (Gillis et al., 2013; Holm et al., 2011). However, it should not be neglected that other studies have suggested a protective role of TGF- β activity in the process of aneurysm development (Bertoli-Avella et al., 2015; Lindsay et al., 2012; van de Laar et al., 2011; Yang et al., 2016).

The TGF- β pathway is mediated through the phosphorylation of and interaction between *Smad2* and *Smad3* and the common interactor *Smad4*, which all form a complex that regulates gene transcription in the nucleus (Shi and Massagué, 2003). Human syndromes resulting from *SMAD4* mutations also include high-frequency aortic aneurysms (Andrabi et al., 2011; Heald et al., 2015; Teekakirikul et al., 2013). Given that *Smad4* is an obligatory component of the canonical TGF- β pathway, targeting its encoding gene has been exploited as a strategy for unraveling the role of TGF- β signaling in aortic pathology. Because whole-genome *Smad4* ablation is embryonically lethal in mice, Zhang et al. recently demonstrated that the conditional deletion of *Smad4* in *Acta2*-expressing smooth muscle cells (SMCs) induces aortic aneurysms (Zhang et al., 2016). Although it informs the causal link between *Smad4* loss of function and aneurysm formation, the pathology developed in these mice is very severe and does not allow thorough investigation of the mechanisms.

To this aim, we induced a targeted deletion of *Smad4* in adult mice by using a tamoxifen-inducible Cre recombinase under the control of the SMC promoter. This study demonstrates a key mechanistic role of structural alterations and immune and inflammatory processes driven by interleukin-1 β (IL-1 β) produced by



(legend on next page)

SMCs in aortic aneurysms deriving from disrupted canonical TGF- β signaling in SMCs. The activation of IL-1 β as a danger signal of SMCs subsequently recruits innate immune cells by activating monocyte chemoattractant protein 1 (MCP-1), also referred to as chemokine (C-C motif) ligand 2 (CCL2), and its cognate receptor C-C chemokine receptor type 2 (CCR2). More important, administration of a neutralizing anti-IL-1 β antibody protects against the evolution of aortic pathology, opening the way to translational therapeutic approaches in aneurysms with compromised canonical TGF- β signaling, such as those driven by *SMAD4* mutations.

RESULTS

Deletion of SMC-Specific *Smad4* in Adult Mice Causes Aneurysmal Formation in the Aorta

To dissect the causal link between defective TGF- β signaling in the vasculature and aneurysm formation, we generated a murine model with SMC-specific deletion of *Smad4*, the common intracellular interactor of canonical TGF- β signaling. To avoid the confounding effects of inactivation of TGF- β signaling during development, we used an inducible Cre-loxP system driven by a smooth muscle myosin heavy chain promoter, *Myh11*, to delete *Smad4* selectively in SMCs of adult mice. We treated *Smad4^{fl/fl};Myh11-creERT2* mice (abbreviated as *Smad4*-SMC in the figures) with tamoxifen to allow Cre-mediated recombination of *Smad4* in SMCs (referred to as *Smad4*-SMC^{iko} mice in the figures), whereas control groups received only vehicle (referred to as *Smad4*-SMC^{WT} mice in the figures). Analysis of *Smad4* in aortas dissected 1 week later showed lower amounts in tamoxifen-treated mice than in animals that had received vehicle alone (Figure S1A). Additional analyses showed that less *Smad4* was specifically detectable in tamoxifen-treated mice carrying the *Smad4* mutation than in mice without the mutation (*Smad4^{+/+};Myh11-creERT2*) (Figure S1A). Immunofluorescence analysis further demonstrated that the deficiency of *Smad4* was confined to the media layer and did not affect the endothelium (Figures S1B and S1C).

Before proceeding with the characterization of aortic pathology, we assessed the general cardiovascular function of tamoxifen-treated *Smad4^{fl/fl};Myh11-creERT2* mice and vehicle-treated *Smad4^{fl/fl};Myh11-creERT2* mice at day 0 and the following time points. Initial (basal) and final (16 weeks) analyses, shown in Table S1, indicated that SMC-specific *Smad4* deletion affected neither blood pressure nor cardiac structure and function. Serial

ultrasonographical analyses of the whole aorta, performed every 4 weeks for up to 16 weeks starting at day 0 after tamoxifen or vehicle administration, revealed that the aortas of *Smad4^{fl/fl};Myh11-creERT2* mice treated with tamoxifen progressively enlarged, whereas none of the vehicle-treated control mice showed any significant variation from their basal condition (Figures 1A–1C).

At gross autoptic examination, all aortas of *Smad4^{fl/fl};Myh11-creERT2* mice treated with tamoxifen displayed one or more evident pathologies, mainly manifested as enlargements and dilations, whereas aortas from *Smad4^{fl/fl};Myh11-creERT2* mice treated with vehicle appeared normal (Figure 1D). Regarding the prevalence of aortic pathologies, we found 100% penetration in *Smad4^{fl/fl};Myh11-creERT2* mice treated with tamoxifen, and the timing of their appearance varied by aortic region (Figure 1E schematically depicts the locations of the aneurysms). The ascending portion of the aorta showed a mildly enlarged diameter at 4 weeks and culminated in the formation of aneurysms at 8 weeks (Figures 1A–1C). Conversely, ultrasonographic monitoring of the abdominal aorta revealed that aneurysms formed later at 12 weeks (Figures 1F–1H). Because of the earliest aneurysmal appearance in the ascending aorta, we focused our mechanistic evaluations on this location throughout the study.

As shown in the Kaplan-Meier plot, the survival of *Smad4^{fl/fl};Myh11-creERT2* mice treated with tamoxifen was severely reduced after *Smad4* deletion, whereas none of the control *Smad4^{fl/fl};Myh11-creERT2* mice treated with vehicle died during the observation time (Figure 1I). In particular, the mortality of *Smad4^{fl/fl};Myh11-creERT2* mice treated with tamoxifen was nearly 30% during the time frame of ultrasonographic analysis (i.e., within 16 weeks after *Smad4* deletion), when mice died of aneurysm rupture, as indicated by the presence of hemothorax at necropsy.

Structural disarrangement of the ascending aorta media in *Smad4^{fl/fl};Myh11-creERT2* mice treated with tamoxifen was clearly appreciated as discrete breaks of elastic lamellae 8 weeks after tamoxifen-induced *Smad4* deletion (Figures 2A–2C). Unlike aortopathies, which are characterized by degenerative changes and identified as cystic medial necrosis (Guo et al., 2001), the islands of damage detected in the aortas of *Smad4^{fl/fl};Myh11-creERT2* mice treated with tamoxifen were not deprived of cells but rather contained groups of cells with spindle-shaped nuclei (Figure S1D). In addition, the sites of break did not show amorphous matrix deposition, as implied by the reduction of

Figure 1. Deletion of SMC-Specific *Smad4* in Adult Mice Determines Aneurysm Formation in Ascending and Abdominal Aortas

(A and B) Representative sequential ultrasound imaging of the ascending aortas of *Smad4*-SMC^{WT} (A) and *Smad4*-SMC^{iko} (B) mice shows progressive vessel dilation and aneurysm formation (n = 9 mice per group). Scale bars, 1 mm.

(C) Ascending aortic diameters of n = 9 mice per group were quantitatively analyzed by ultrasound imaging. Two-way ANOVA for repeated measures: df = 4, $F_{(\text{interaction})} = 67.80$.

(D) Anterior view of the thoracic cavity shows heart and great vessels of mice 16 weeks after treatment with vehicle (top) or tamoxifen (bottom). Aneurysms are clearly visible on the lateral side of the ascending aorta in *Smad4*-SMC^{iko} mice.

(E) Schematic representation of the entire aorta shows the different segments analyzed and indicates the locations where aneurysms developed (black arrows) in *Smad4*-SMC^{iko} mice.

(F and G) Progression of abdominal aorta pathology in *Smad4*-SMC^{iko} mice (G) and control mice (F). Scale bars, 1 mm.

(H) Quantitative analysis of abdominal aortic diameters of n = 9 mice per group. Two-way ANOVA for repeated measures: df = 4; $F_{(\text{interaction})} = 16.34$.

(I) Kaplan-Meier plot for *Smad4*-SMC^{iko} (n = 17) and *Smad4*-SMC^{WT} (n = 15) mice shows significantly increased mortality after *Smad4* deletion. Log rank test: df = 1, $\chi^2 = 34.62$, p < 0.0001. *p < 0.05, **p < 0.01, ***p < 0.001.

Please also see Figures S1A–S1C, S7A, and S7B.

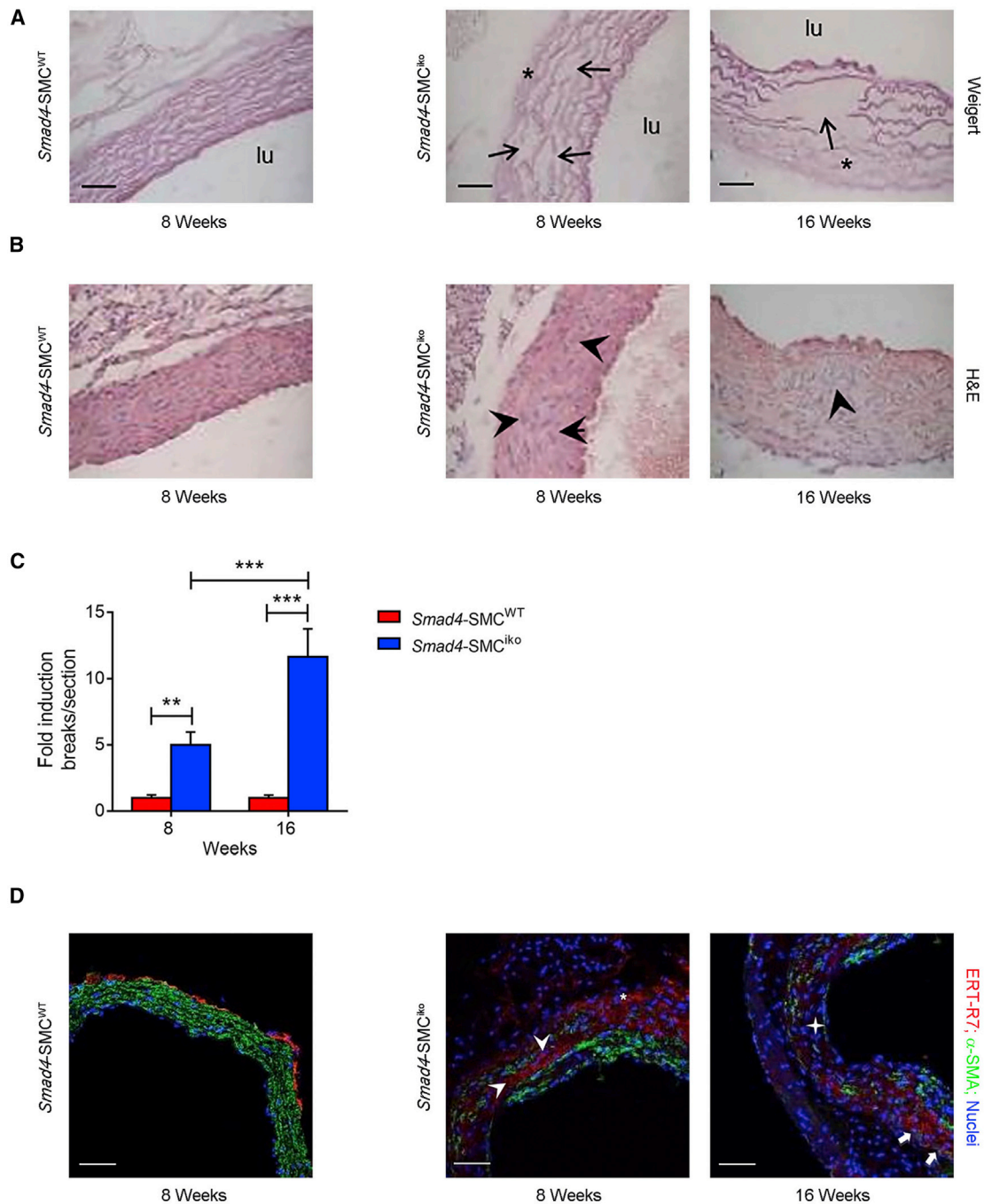


Figure 2. Deletion of SMC-Specific *Smad4* in Adult Mice Determines Disarrangement of Aortic Wall

(A and B) Staining of consecutive sections of ascending aorta with Weigert reagent (A) or hematoxylin and eosin H&E (B). Elastic lamellae breaks are indicated by arrows in sections stained with Weigert reagent; the corresponding sites in H&E-stained sections are marked by arrowheads. Scale bars, 50 μ m.

(C) Quantitation of breaks of elastic lamellae in ascending aorta. $n = 11$ mice per group at 8 weeks and 4 mice per group at 16 weeks. Two-way ANOVA: $df = 1$; $F_{(\text{interaction})} = 10.30$; $**p < 0.01$, $***p < 0.001$.

(D) Remodeling of the wall structure of ascending aorta. Representative sections of ascending aortas from 11 mice per group at 8 weeks and 4 mice per group at 16 weeks were stained with antibodies to α -SMA and ER-TR7, an antigen expressed by adventitial fibroblasts. Scale bars, 50 μ m.

Please also see [Figures S1D–S1H](#).

histochemical staining for mucopolysaccharides ([Figures S1E and S1F](#)). Immunostaining for collagen I in lamellae breaks was lower in the media of *Smad4^{fl/fl};Myh11-creERT2* mice treated with

tamoxifen than in that of control *Smad4^{fl/fl};Myh11-creERT2* mice treated with vehicle ([Figures S1G and S1H](#)). With time, the severity of damage increased ([Figures 2A–2C](#), 16 weeks),

and zones with staked fragmentations of elastic lamellae became apparent (Figure 2A, 16 weeks, arrow).

In the adventitia of the aortas of *Smad4^{fl/fl};Myh11-creERT2* mice treated with tamoxifen, structural remodeling also determined a thickening of this layer (asterisks in Figure 2A) and, at some sites, penetration of cells into the media. This process could be followed by staining of adventitial fibroblasts and media with antibody to ER-TR7 and α -smooth muscle actin (α -SMA) (Figure 2D). In control mice, a thin layer of ER-TR7⁺ cells marked the adventitia, whereas the media uniformly expressed α -SMA (Figure 2D). However, 8 weeks after *Smad4* deletion, the ER-TR7⁺ cells were detected in the thickened adventitia (asterisk in Figure 2D) and were also found among SMCs (arrowheads in Figure 2D). When alterations of elastic lamellae were more severe, most cells appeared negative for both α -SMA and ER-TR7 expression (star in Figure 2D, 16 weeks), whereas some staining remained at the border of these sites (thick arrows in Figure 2D, 16 weeks).

8 weeks after *Smad4* deletion in SMCs, adventitial inflammation was clearly present in those regions of the media with fragmentation of elastic lamellae. The immune infiltrate (Figure 3A) was composed mainly of monocyte and macrophages, as indicated by the abundance of CD11b⁺ (Figure 3B) and CD68⁺ (Figure 3C) cells and the near absence of lymphocytes (CD3 staining in Figure S1I). Adventitial gathering of immune cells was always found in locations of the media with discrete stacked breaks of elastic lamellae, indicating a strict association between damage of the media and the presence of inflammatory infiltrate in the adventitia. In accordance, flow-cytometric analysis of cells from aortas isolated 8 weeks after tamoxifen treatment detected a significantly increased number of infiltrating leukocytes gated as CD45⁺ and marked as CD11b⁺ Ly6C^{high} monocytes and CD11b⁺ Ly6C^{low} macrophages (Figures 3D–3I).

Disruption of TGF- β Signaling Induces Early Mechanical Alterations of the Aorta with No Overt Sign of Inflammation

Growth of aortic aneurysms is a process typically accompanied by increased circumferential wall stress (Raaz et al., 2015). Even though wall stress is usually believed to surge as a consequence of the vessel's expanding geometry, contributing to the eventual rupture of advanced aneurysms, it is also conceivable that enhanced circumferential wall stress occurs because of early biomechanical alterations at pre-aneurysmal stages, thus contributing to the etiology of the disease itself. On this note, aortic aneurysms usually display a mechanical behavior different from that of non-aneurysmal tissue (He and Roach, 1994), and immune response in tissue remodeling participates in this process (Daugherty and Powell, 2014; Jagadesham et al., 2008). To find out whether changes in mechanical properties and recruitment of immune response are early events of the pathogenetic cascade triggered by *Smad4* inactivation and not a simple consequence of aortic disarrangement accompanying aneurysm formation, we investigated both mechanics and immune response at a time point preceding the signs of aneurysm formation, i.e., 3 weeks after tamoxifen or vehicle administration, when aortic diameters measured by ultrasound imaging were still comparable between the two groups (Figure S2A).

To test the intrinsic mechanical properties of the aorta after *Smad4* deletion, we excised the ascending portion of the vessel and mounted it on a pressure myograph. We analyzed the structural and functional parameters by subjecting vessels to increasing perfusion pressures. Ascending aorta segments exhibited increased outer (Figure 4A) and inner (Figure S2B) diameters at increasing perfusion pressure steps. Wall thickness (Figure S2C) and the wall-to-lumen ratio (Figure 4B) decreased, reaching statistical significance at low intraluminal pressures. Although modifications of the above parameters increased circumferential wall stress (Figure S2D), circumferential strain (Figure S2E) was comparable between vessels from mutant and control animals. Relevant to this last observation, the stress-strain curves showed significantly more aortic stiffness in *Smad4^{fl/fl};Myh11-creERT2* mice treated with tamoxifen than in *Smad4^{fl/fl};Myh11-creERT2* mice treated with vehicle (Figure 4C). Accordingly, the incremental elastic modulus, an intrinsic vessel property independent from the geometry, was increased at high pressures (Figure 4D). At the microstructural level, alterations of the vessel wall were detectable as well, as surmised by the presence of elastic lamellae breaks even 3 weeks after *Smad4* deletion (Figures 4E–4G).

The above data clearly show that modifications of the mechanical properties of the aorta are an early event in aneurysm formation, suggesting that *Smad4* inactivation could impinge on the expression of genes relevant for structural stability and functional performance of the vessel. Given that *Smad*-dependent TGF- β signaling has been identified as a major determinant of differentiation and functional phenotype of SMCs, as well as extracellular matrix (ECM) setup and cell adhesion (Guo and Chen, 2012), we performed analyses on genes involved in these functions. The expression of several cytoskeletal genes was similar between *Smad4^{fl/fl};Myh11-creERT2* mice treated with tamoxifen and those treated with vehicle (Figure S2F). Moreover, the phosphorylation of MLC20 and MYPT1, major regulators of SMC contractility and calcium sensitivity, respectively, was also comparable between the two groups (Figure S2G). On the other hand, investigation of genes involved in the ECM and cell adhesion revealed some differences. Among numerous genes analyzed, expression of the following six genes varied significantly between control mice and mice with a *Smad4* deletion: *Eln*, *Col1a1*, *Lox* (ECM and its metabolism), *Itga2* (collagen receptor), and *Pxl* and *Vcl* (focal adhesion components) (Figure S2H). However, no changes in the transcripts of different proteases were noted (Figure S2I).

Smad4 Signaling Negatively Regulates IL-1 β Production in SMCs

In addition, analysis of several cytokines and chemokines revealed that the inactivation of *Smad4* increased SMC transcripts of IL-1 β , IL-6, and CCL2 while reducing those of IL-4, CXCL10, interferon- γ (IFN- γ), and IFN- β (Figure 5A). It is worth noting that the observed changes were most likely related to genes expressed in SMCs of the media, given that the adventitia was carefully removed. On the other hand, this was not surprising because it is well known that IL-1 β , despite being produced at high concentrations in stimulated macrophages, was found to be upregulated also in aortic SMCs in human thoracic aneurysms (Johnston et al., 2014). IL-1 β is produced and stored in cells as an inactive precursor, and the release in its active form

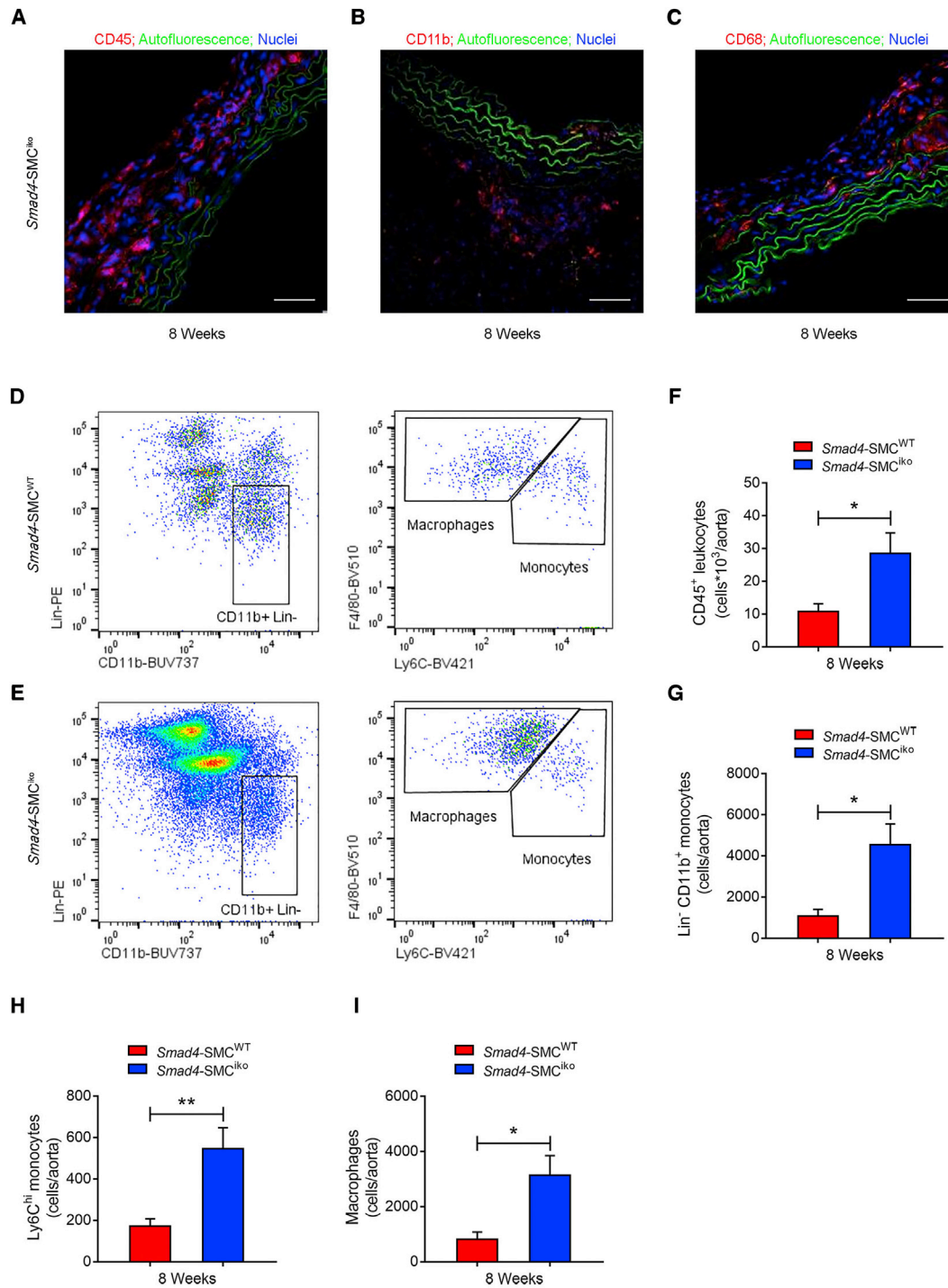


Figure 3. Smad4 Deficiency in SMCs Determines a Progressive Recruitment of Monocytes and Macrophages in the Aortic Wall

(A–C) Sections from the ascending aortas of *Smad4-SMC^{ko}* and *Smad4-SMC^{WT}* mice 8 weeks after tamoxifen treatment were stained with different hematopoietic cell markers. Strong staining for CD11b (B) and CD68 (C) indicates that most adventitial cells of hematopoietic origin (CD45) (A) are monocytes and macrophages. Scale bars, 50 μ m.

(D–I) Flow-cytometric gating in *Smad4-SMC^{ko}* (E) and *Smad4-SMC^{WT}* (D) mice and quantification of aortic leukocytes (F–I). $n = 6$ *Smad4-SMC^{WT}* mice and 8 *Smad4-SMC^{ko}* mice. Student's t test for independent samples: (F) $t_{(8,780)} = -2.639$, (G) $t_{(8,333)} = -3.246$, (H) $t_{(8,735)} = -3.505$, and (I) $t_{(8,834)} = -3.095$; * $p < 0.05$ and ** $p < 0.01$.

Please also see [Figures S11](#) and [S7C](#).

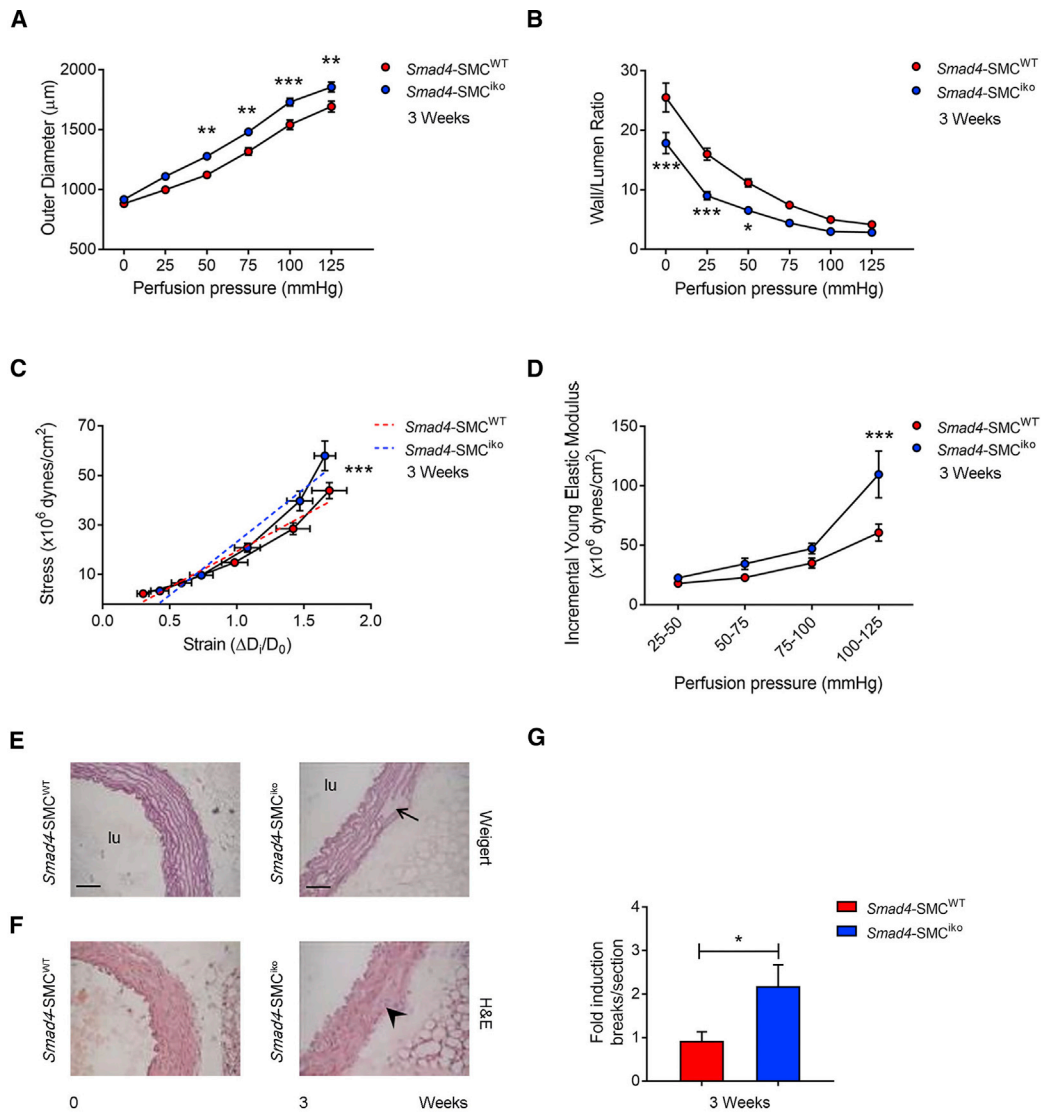


Figure 4. Alterations of Biomechanical Functions of the Aorta Precede the Appearance of Aneurysm

(A–D) Segments of ascending aorta were dissected 3 weeks after *Smad4* deletion, mounted on a pressure myograph, and subjected to increasing perfusion pressure for determining the following parameters: outer diameter (A), wall-to-lumen ratio (B), stress-strain relationship showing aortic stiffness (C), and incremental young elastic modulus (D). $n = 11$ *Smad4-SMC^{WT}* mice and 7 *Smad4-SMC^{iko}* mice. Two-way ANOVA for repeated measures: (A) $df = 5$, $F_{(\text{interaction})} = 5.763$; (B) $df = 5$, $F_{(\text{interaction})} = 3.773$; and (D) $df = 3$, $F_{(\text{interaction})} = 5.775$. Dashed lines in (C) represent the slopes of stress-strain curves, and their differences were tested by linear regression analysis ($df = 1$, $F_{(\text{interaction})} = 13.671$). * $p < 0.05$, ** $p < 0.01$, *** $p < 0.001$.

(E and F) Staining of consecutive sections of ascending aorta with Weigert reagent (E) or H&E (F). Elastic lamellae breaks started to appear 3 weeks after *Smad4* deletion. Scale bars, 50 μm .

(G) Quantitation of breaks of elastic lamellae in ascending aorta: $n = 7$ *Smad4-SMC^{WT}* mice 9 *Smad4-SMC^{iko}* mice. Mann-Whitney test for independent samples: * $p < 0.05$.

Please also see Figure S2.

requires caspase-1 cleavage. In turn, in order to be activated, caspase-1 requires the function of NLRP3, a sensor that is an essential component of the NLRP3 inflammasome, a multiprotein platform that assembles in response to infection and tissue damage to allow the activation of inflammatory caspases (Schroder and Tschopp, 2010). Therefore, we tested NLRP3 mRNA amounts and found them to be significantly higher in *Smad4^{fl/fl};Myh11-creERT2* mice treated with tamoxifen than in control mice (*Smad4^{fl/fl};Myh11-creERT2* mice treated with

vehicle) (Figure 5A). When we looked for infiltrating immune cells by flow-cytometric analysis 3 weeks after tamoxifen, we did not find increased CD45⁺ leukocytes or, more specifically, CD11b⁺ monocytes (Figures S3A–S3D), suggesting that immune reaction surged later and further supporting the concept that IL-1 β should be activated in SMCs as a danger signal.

To provide additional evidence that deletion of *Smad4* in SMCs determined an upregulation of IL-1 β in a cell-autonomous way, we analyzed and quantified by confocal microscopy the

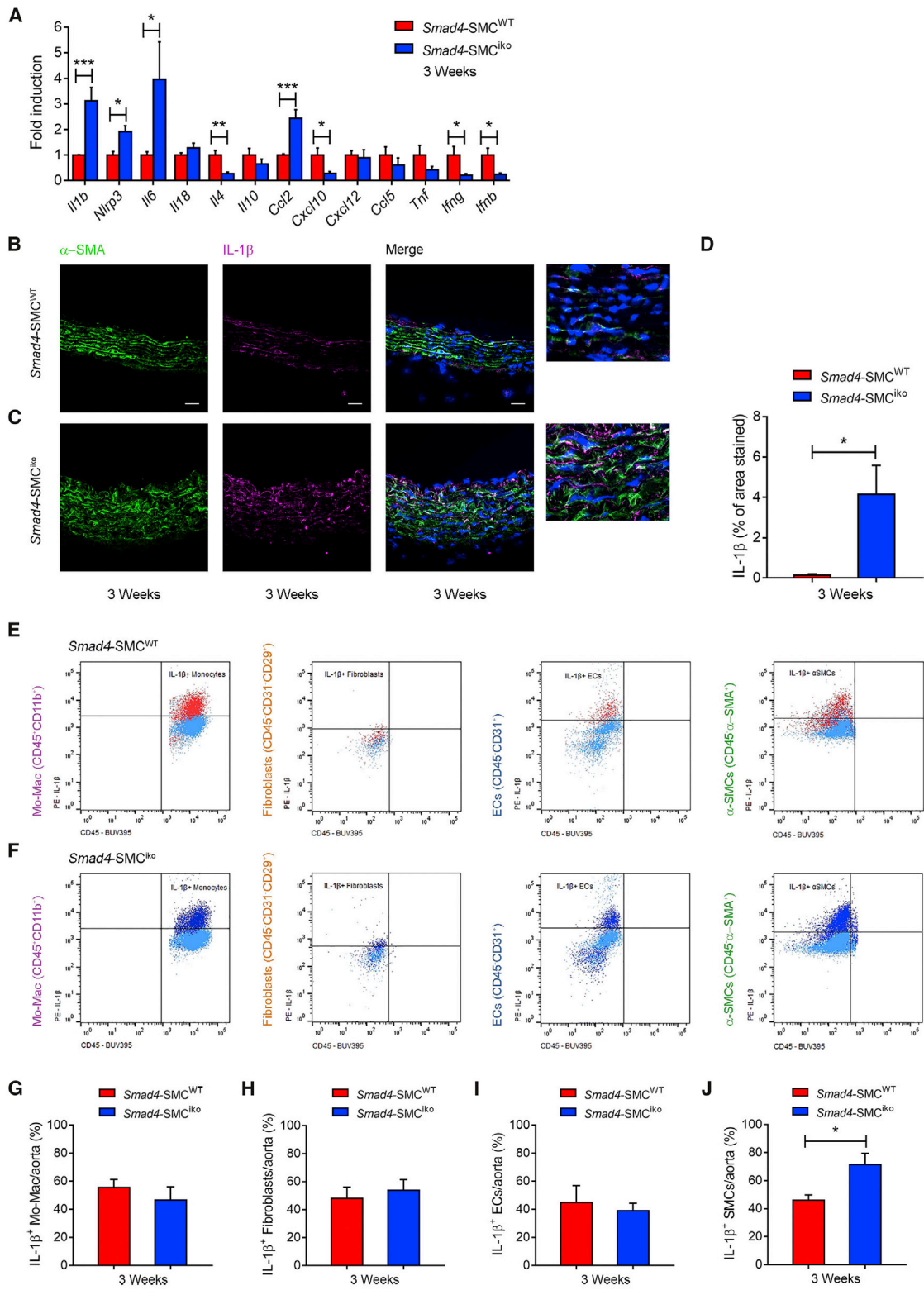


Figure 5. *Smad4* Ablation in SMCs Activates Inflammation Early in the Media and Induces IL-1 β Production

(A) Ascending aortas were collected 3 weeks after tamoxifen or vehicle administration, the adventitia was carefully removed, and the media were processed for RNA purification and qRT-PCR analysis. Analysis of several cytokine and chemokine gene transcripts showed significant variation for those encoding IL-1 β , IL-6, and CCL2 (upregulated) and those encoding IL-4, CXCL10, IFN- γ , and IFN- β (downregulated). Transcripts of the inflammasome component NLRP3 were also

(legend continued on next page)

percentage of IL-1 β immunofluorescence in the SMC area labeled with α -SMA (Figures 5B–5D). Similarly, flow-cytometric analysis of single-cell suspensions prepared from the aortas of *Smad4^{fl/fl};Myh11-creERT2* mice treated with tamoxifen and *Smad4^{fl/fl};Myh11-creERT2* mice treated with vehicle revealed that the inhibition of TGF- β signaling increased the percentage of IL-1 β ⁺ cells specifically in the SMC fraction, obtained by gating of CD45⁻CD31⁻ and α -SMA⁺ cells (Figures 5E–5J).

We next looked at the mechanisms responsible for the upregulation of IL-1 β in SMCs, determined by the deletion of *Smad4*. As first, we assessed the possibility that IL-1 β could be directly upregulated in SMCs and, to this aim, exploited a typical pro-inflammatory stimulus known to regulate the expression of this cytokine, namely lipopolysaccharide (LPS), the bacterial endotoxin activating Toll-like receptor 4 (TLR4). The *in vitro* stimulation of SMCs with LPS strongly upregulated the mRNA amounts of the main cytokines that we found upregulated in the vessels deficient in *Smad4* signaling and deprived of the adventitia layer: IL-1 β , IL-6, and CCL2 (Figures S3E–S3G). To unravel the specific role of TGF- β signaling in modulating IL-1 β production in SMCs in the more complex context of whole aortic tissue, we directly stimulated pressurized vessels with LPS in the presence or absence of TGF- β and assessed IL-1 β -producing cells by flow cytometry. As shown in Figures S3H and S3I, the percentage of IL-1 β ⁺ cells on SMC gating was significantly increased upon LPS stimulation. The concomitant incubation of vessels with TGF- β significantly hampered the LPS-mediated IL-1 β production, whereas TGF- β alone had no significant effect (Figures S3H and S3I). Similar results were obtained when vessels were incubated with the same protocol and analyzed by confocal microscopy after immunofluorescence staining (Figures S3J and S3K).

Together, these data suggest to us that, in principle, TGF- β signaling in SMCs is able to negatively regulate IL-1 β when challenged by stimuli such as LPS. To put this observation in the context of the phenotype observed in *Smad4^{fl/fl};Myh11-creERT2* mice treated with tamoxifen, we attempted to mimic the effect of genetic deletion of *Smad4* in the simpler experimental system of pressurized isolated vessels. When aortas from wild-type mice were incubated with the TGF- β RI inhibitor SB525334, IL-1 β was markedly increased in SMCs (Figures S4A–S4C), thus supporting the concept that TGF- β signaling through *Smad4* directly acts as an inhibitor of IL-1 β .

IL-1 β Activates an Autocrine Pathway in SMCs with a Central Role in the Aortic Pathology of Mice with Inducible *Smad4* Deletion in SMCs

Smad4 inactivation is expected to block the transcriptional response stimulated by the canonical TGF- β and bone morpho-

genetic protein (BMP) pathways. However, in the absence of *Smad4*, TGF- β receptors remain functionally intact and continue to signal through other paths collectively referred to as non-Smad (non-canonical) signaling (Mu et al., 2012). These pathways are considered to be of pathogenetic importance for aortic aneurysms with dysregulation of TGF- β signaling, such as those found in Marfan syndrome and LDS. We therefore analyzed the phosphorylation of kinases and regulatory Smads that might take part in non-canonical TGF- β signaling. Silenced *Smad4* was accompanied by increased phosphorylation of Smad2/3 and Smad1/5/8 (Figures S4D and S4E). However, expression of TGF- β and BMP target genes was not affected (Figure S4F). Moreover, except for *Smad4* transcript reduction, no variations were detected for other components of the two pathways (Figures S4G and S4H). More important, amounts of phosphorylated Erk1/2, p38, and JNK mitogen-activated protein kinase (MAPK) (Figures S4I and S4J) and PKB, also referred to as Akt (data not shown), remained unaltered, thus ruling out the activation of these non-canonical TGF- β pathways. We also tested activation of TGF- β -activated kinase 1 (TAK-1), another MAPK whose activation by TGF- β does not require kinase activity of TGF- β receptors (Mu et al., 2012). Although we found no variation in TAK-1 phosphorylation (Figures S4K and S4L), to our surprise, we detected significantly increased phosphorylation of a potential downstream signaling component, NF- κ B, specifically the RelA subunit, also known as p65 (Figures S4K and S4L). NF- κ B is a transcriptional complex regulated by stimuli such as various types of stress, and it controls a large variety of target genes, several of which are involved in inflammation (Hayden and Ghosh, 2012). Thus, the increase in P-RelA in SMCs indicates that NF- κ B might contribute to the aortic phenotype of *Smad4* mutants by inducing modification of the expression of several cytokines and chemokines (Figure 5A). In turn, some inflammatory cytokines, including IL-1 β , have been reported to affect collagen biosynthesis in various types of SMCs (Amento et al., 1991; Aoki et al., 2009), thus suggesting that the early mechanical alterations of the vessel and later concomitant recruitment of immune response could be two sides of the same phenomenon—a molecular mechanism activated by *Smad4* deletion.

The above results suggest that NF- κ B and IL-1 β might be involved in aneurysm formation due to *Smad4* deletion in SMCs. IL-1 β can be induced by NF- κ B, but it is also an activator of NF- κ B (Hiscott et al., 1993; Weber et al., 2010), hinting at the possibility that positive feedback between the two components might aggravate aneurysm progression. In relation to this issue, we assessed the expression of IL-1 receptor (IL-1R) in the aortas of *Smad4^{fl/fl};Myh11-creERT2* mice treated with vehicle or

increased. Student's t test for independent samples ($n = 3$ – 8 mice) was applied for *Il4* ($t_{(8)} = 3.835$), *Cxcl12* (not significant [ns]), *Ccl5* (ns), *Ifng* ($t_{(8)} = 2.302$), and *Ifnb* ($t_{(8)} = 2.734$). A Mann-Whitney test for independent samples was applied for *Il1b*, *Nlrp3*, *Il6*, *Il18*, *Il10*, *Ccl2*, *Cxcl10*, and *Tnf*.

(B–D) Representative images of IL-1 β immunofluorescent staining in ascending aortas of *Smad4*-SMC^{WT} ($n = 5$) (B) and *Smad4*-SMC^{ko} ($n = 6$) (C) mice. Scale bars, 20 μ m. Staining was quantified as the relative fluorescence intensity normalized to the media layer area and identified as α -SMA⁺ cells (D). Mann-Whitney test for independent samples: * $p < 0.05$.

(E–J) Aortic cell suspensions from the aortas of *Smad4*-SMC^{WT} (E) and *Smad4*-SMC^{ko} (F) mice were stained with anti-CD45, CD11b, CD31, α -SMA, CD29, and IL-1 β antibodies or an appropriate isotype control and assessed by flow cytometry. Representative IL-1 β staining (red *Smad4*-SMC^{WT} and blue for *Smad4*-SMC^{ko}) of hematopoietic (CD45⁺CD11b⁺) cells, nonhematopoietic vascular cells, gated endothelial cells (ECs), fibroblasts, and SMCs is shown. The corresponding isotype control for IL-1 β (light blue) within each gate is shown. The percentage of IL-1 β positivity within each subset was quantified (G–J). $n = 4$ mice per group. Student's t test for independent samples: Mo-Mac (G, ns), fibroblasts (H, ns), ECs (I, ns), and SMCs (J, $t_{(8)} = 2.860$); * $p < 0.05$.

Please also see Figures S3, S4, and S7D–S7F.

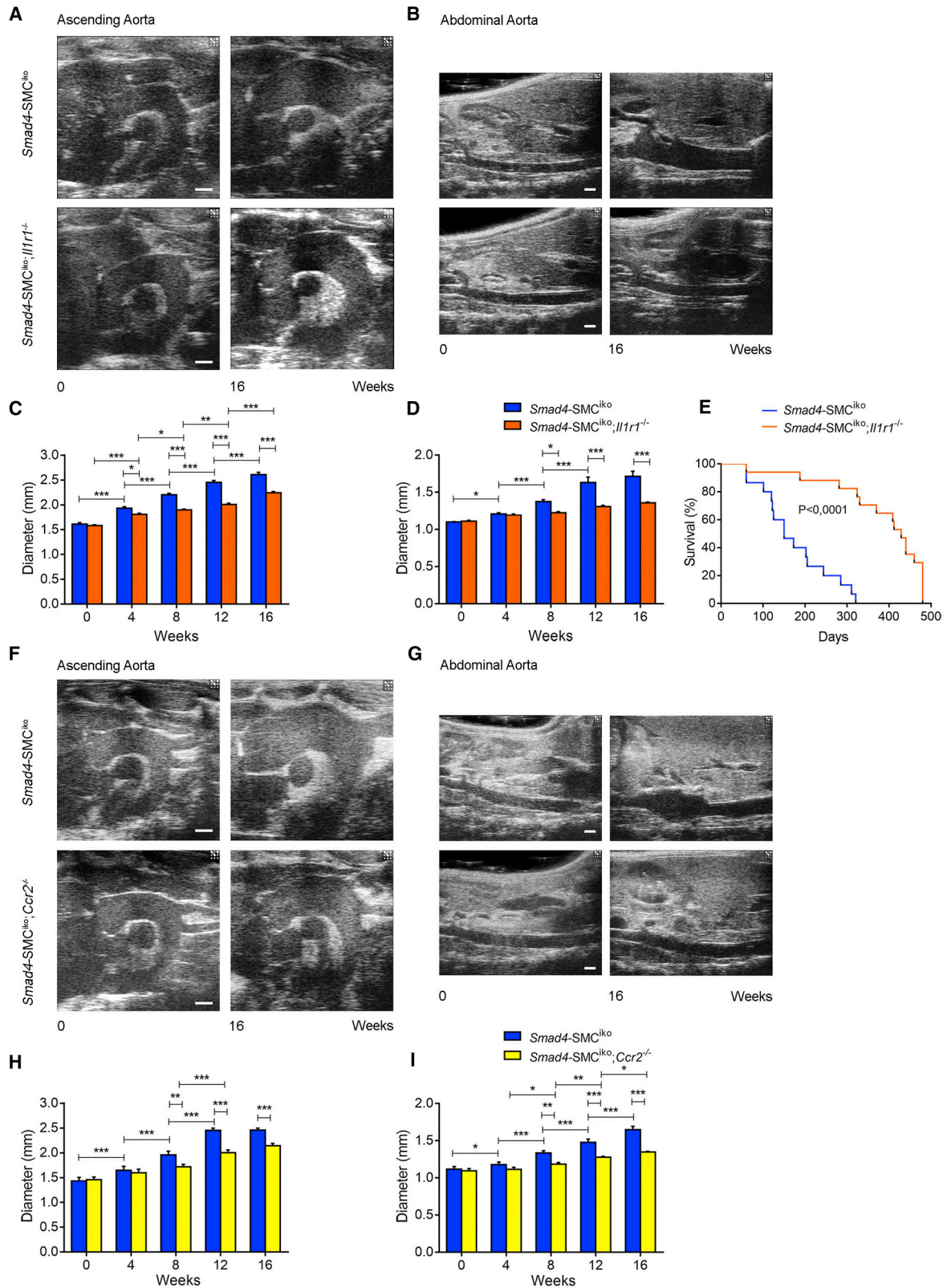


Figure 6. Inhibition of the IL-1 β -CCL2 Axis Hampers Progression of Aortic Aneurysm in Mice with SMC-Specific *Smad4* Deletion

(A and B) Representative ultrasound imaging of the ascending (A) and abdominal (B) aortas of *Smad4-SMC^{ik0}* and *Smad4-SMC^{ik0}; Il1r1^{-/-}* mice shows significant protection from vessel dilation and aneurysm formation in mice with an *Il1r1*-null background. Scale bars, 1 mm.

(legend continued on next page)

tamoxifen and found a strong colocalization in SMCs (Figures S5A and S5B). Supporting the hypothesis of an autocrine mechanism regulated by positive feedback of IL-1 β in SMCs, we found that direct stimulation of SMCs with IL-1 β was able to increase the expression of the cytokine itself (Figure S5C). In the same setting, IL-1 β stimulation was also able to increase the expression of *Il6* and the chemokine *Ccl2* in SMCs (Figures S5D and S5E), suggesting an apical role of IL-1 β signaling in inflammation and activation of the immune response.

Therefore, we reasoned that blocking IL-1R might dampen IL-1 β signaling and have a beneficial effect on morphological alterations of aneurysms. We tested this hypothesis by inducing *Smad4* deletion in SMCs of mice with an *Il1r1*-null background (*Smad4^{fl/fl};Myh11-creERT2;Il1r1^{-/-}* mice treated with tamoxifen). Serial ultrasonographic analyses revealed that ablation of *Il1r1* protected from pathology progression in the ascending aorta and the abdominal part (Figures 6A–6D). Further supporting the protective role of IL-1 inhibition, Kaplan-Meier analysis showed that *Il1r1* ablation increased survival of *Smad4^{fl/fl};Myh11-creERT2;Il1r1^{-/-}* mice treated with tamoxifen (Figure 6E). Overall, these results suggest that increased IL-1 signaling is a central event following *Smad4* inactivation.

We next tested whether the increase in P-RelA was due to activation of the IL-1 pathway or was independent from it. RelA phosphorylation was analyzed by immunoblotting in the aortas of tamoxifen-treated *Smad4^{fl/fl};Myh11-creERT2* mice with or without the *Il1r1*-null mutation. P-RelA was significantly more inhibited in tamoxifen-treated *Smad4^{fl/fl};Myh11-creERT2* mice carrying the *Il1r1^{-/-}* mutation than in tamoxifen-treated *Smad4^{fl/fl};Myh11-creERT2* mice without the mutation (Figures S5F and S5G), suggesting that NF- κ B activation in the media is dependent on IL-1 β signaling and not vice versa. In addition, we found that the increased expression of *Ccl2* and *Nlrp3* in the aortas of *Smad4^{fl/fl};Myh11-creERT2* mice treated with tamoxifen was rescued in the *Il1r1^{-/-}* background, whereas the reduced expression of *Il4*, *Ifnb*, and *Ifnb* transcripts was normalized (Figure S5H), suggesting that these genes were downstream of IL-1 β . Deletion of *Il1r1* also brought transcripts for *Eln*, *Col1a1*, *Lox*, *Itga2*, *Pxn*, and *Vcl* back to normal amounts (Figure S5H). Thus far, these data suggest that IL-1 β has a key role not only in the control of cytokines that determine inflammation but also in the expression of genes important for ECM stability and cell adhesion. Further supporting this last observation, we also found that tamoxifen-treated *Smad4^{fl/fl};Myh11-creERT2* mice on the *Il1r1^{-/-}* background were significantly protected from the progressive break of elastic lamellae that occurred in *Smad4^{fl/fl};Myh11-creERT2* mice treated with tamoxifen (Figures S5I and S5J).

To appreciate fully the pathophysiological impact of IL-1 β targeting on the aortic disease, we assessed *in vivo* mechanical

properties by echo-tracking the wall motion on ultrasound images. We extracted data relative to arterial stiffness and distensibility. *Smad4^{fl/fl};Myh11-creERT2* mice treated with tamoxifen showed a significantly increased index of arterial stiffness, which was already evident 4 weeks after gene inactivation and continued to worsen at the last time point (Figure S5K). At the same time, *Smad4^{fl/fl};Myh11-creERT2* mice treated with tamoxifen displayed less distensibility of the aorta than mice treated with vehicle (Figure S5L). The inhibition of IL-1 β signaling, obtained in tamoxifen-treated *Smad4^{fl/fl};Myh11-creERT2* mice with the *Il1r1^{-/-}* mutation, realized complete protection from the mechanical alterations observed in *Smad4^{fl/fl};Myh11-creERT2* mice treated with tamoxifen (Figures S5K and S5L). These results appear particularly important because they further support a protective effect of IL-1 β inhibition on pathology progression in *Smad4^{fl/fl};Myh11-creERT2;Il1r1^{-/-}* mice treated with tamoxifen, despite the moderately increased aortic diameter displayed with time progression (Figures 6A–6D).

Inhibition of the CCL2-CCR2 Chemokine Axis Blocks Pro-inflammatory Monocyte Infiltration and Ameliorates Aneurysm Progression

The fact that IL-1 β was upregulated before infiltration of monocytes and macrophages (Figures 5A and S3A–S3D) suggests that this cytokine plays a role in transferring signals from the aortic walls to the immune system, which is later activated. On the other hand, IL-1 β was able to induce the expression of *Ccl2* in SMCs (Figure S5E), and the peaking of *Ccl2* observed 3 weeks after tamoxifen treatment in *Smad4^{fl/fl};Myh11-creERT2* mice was rescued when the deletion of *Smad4* was induced in mice with IL-1R deficiency (Figure S5H). Given that Ly6C^{high} pro-inflammatory monocytes typically express high amounts of CCR2 (a receptor of CCL2), we hypothesized that the migration of this subset of monocytes, later found infiltrated in the aortic walls of *Smad4^{fl/fl};Myh11-creERT2* mice treated with tamoxifen, could be regulated through this pathway. Thus, we generated another murine model to induce the ablation of *Smad4* in SMCs of CCR2-deficient mice (*Smad4^{fl/fl};Myh11-creERT2;Ccr2^{-/-}* mice treated with tamoxifen), thus making them unable to respond to CCL2-induced migration of Ly6C^{high} pro-inflammatory monocytes. Resembling *Smad4^{fl/fl};Myh11-creERT2;Il1r1^{-/-}* mice treated with tamoxifen, *Smad4^{fl/fl};Myh11-creERT2;Ccr2^{-/-}* mice treated with tamoxifen displayed a slower progression of aortic aneurysm with a significantly reduced diameter both in the ascending and in the abdominal tracts (Figures 6F–6I). However, unlike tamoxifen-treated *Smad4^{fl/fl};Myh11-creERT2;Il1r1^{-/-}* mice that manifested early protection from structural damage in the aorta (Figure S5I), *Smad4^{fl/fl};Myh11-creERT2;Ccr2^{-/-}* mice treated with tamoxifen

(C and D) Ascending (C) and abdominal (D) aortic diameters were quantitatively analyzed by ultrasound imaging (n = 9 mice per group). Two-way ANOVA for repeated measures: df = 4; $F_{(interaction)} = 23.82$ (ascending aorta) and 16.03 (abdominal aorta).

(E) Kaplan-Meier plot for *Smad4*-SMC^{iko} (n = 17) and *Smad4*-SMC^{iko}; *Il1r1^{-/-}* (n = 17) mice shows that IL-1 inhibition significantly reduced mortality after *Smad4* deletion. Log rank test: df = 1, $\chi^2 = 24.72$, p < 0.0001.

(F and G) Representative ultrasound imaging of the ascending (F) and abdominal (G) aortas of *Smad4*-SMC^{iko} and *Smad4*-SMC^{iko}; *Ccr2^{-/-}* mice (n = 5 per group) shows significant protection from vessel dilation and aneurysm progression in mice with a *Ccr2*-null background. Scale bars, 1 mm.

(H and I) Quantitative analysis of ascending (H) and abdominal (I) aortic diameters. Two-way ANOVA for repeated measures: df = 4; $F_{(interaction)} = 8.929$ (ascending aorta) and 19.90 (abdominal aorta); *p < 0.05, **p < 0.01, ***p < 0.001.

Please also see Figure S5 and S6.

started to display the breaks in the elastic lamellae of the vessels 3 weeks after the deletion of *Smad4* (Figure S6A). Together, these observations suggest that the initial damage in the elastic lamellae of the aorta, despite relying on the activation of IL-1 β , was independent from the infiltration of inflammatory monocytes recruited through the downstream activation of CCL2. This conclusion is also in line with the additional evidence showing that early upregulation of IL-1 β in SMCs was still observed in mice where deletion of *Smad4* was induced in a CCR2-deficient background (Figures S6B–S6D).

We also analyzed the infiltrating immune cells at 8 weeks, when aortas from *Smad4^{fl/fl};Myh11-creERT2* mice treated with tamoxifen were densely enriched with monocytes and macrophages (Figure 3), and found a significant reduction of Ly6C^{high} pro-inflammatory monocytes in *Smad4^{fl/fl};Myh11-creERT2;Ccr2^{-/-}* mice treated with tamoxifen, despite the still increased number of Ly6C^{low}F4/80^{hi} macrophages (Figures S6E–S6H). These results show that the recruitment of classical pro-inflammatory monocytes, depending on the CCL2 signaling, was efficiently blocked by CCR2 inactivation, whereas mobilization of intermediate monocytes and non-classical macrophages was not completely compromised, given that it typically does not rely on the CCL2-CCR2 axis.

Therapeutically Targeting IL-1 β Signaling Improves Aortic Pathology in *Smad4^{fl/fl};Myh11-creERT2* Mice Treated with Tamoxifen

To test the translational potential of our findings, we neutralized IL-1 β signaling with the clinically relevant murine version of the FDA-approved clinical drug canakinumab. After tamoxifen administration, used to induce SMC deletion of *Smad4*, treatment with anti-IL-1 β or control immunoglobulin (CTRL IgG) began and was repeated every week. During a time course of 16 weeks, whereas administration of CTRL IgG did not change aneurysm progression, treatment with anti-IL-1 β antibody significantly hampered aneurysm formation in both ascending and abdominal tracts of the aorta (Figures 7A–7D). The above data not only add support to the mechanistic role of IL-1 β in the aortic pathology induced by SMC deletion of *Smad4* but also identify treatment with IL-1 β inhibitors as potential pharmacological therapy of the disease.

DISCUSSION

Pieces of literature consistently associate disrupted TGF- β signaling with the development of aortic aneurysms. Yet, the molecular mechanisms mediating this association remain to be identified. Our results provide evidence that IL-1 β has an important role in triggering aneurysm formation in a model of aortopathy induced by postnatal deletion of *Smad4* in SMCs. Indeed, we found that genetic inhibition of the IL-1 β pathway significantly hampered progression of aneurysms in *Smad4^{fl/fl};Myh11-creERT2* mice treated with tamoxifen. More important, blocking IL-1 signaling in *Smad4^{fl/fl};Myh11-creERT2* mice treated with tamoxifen reduced the rate of death by aneurysm rupture. To highlight the potential translational use of IL-1 pathway inhibitors, we selectively neutralized IL-1 β with the murine version of an antibody that has recently emerged as an effective treatment for secondary prevention of cardiovascular events in the large-

scale clinical trial CANTOS (Ridker et al., 2017). The results showed a significant protection from aneurysm progression in both ascending and abdominal aorta, hence opening the door to translational perspectives for limiting aortic *Smad4*-dependent aneurysm pathology with an already clinically approved drug. This adds to the protective role of IL-1 β inhibition previously described in experimentally induced cerebral arterial, abdominal aortic, and thoracic aortic aneurysms (Johnston et al., 2014; Johnston et al., 2013; Moriwaki et al., 2006).

Our data show that *Smad4* is required in SMCs for the maintenance of normal aortic structure and function. In particular, we provide evidence that downregulation of *Smad4* stimulates IL-1 β expression in SMCs and that this cytokine regulates the function of several other genes, including those encoding other cytokines and chemokines and components of the ECM and its metabolism and focal adhesions.

The finding that that expression of other cytokines is normalized in the *Il1r1^{-/-}* background indicates that IL-1 β is instrumental for the altered expression of cytokines and chemokines observed in the media early after the induction of *Smad4* inactivation. Among upregulated cytokines and chemokines, CCL2 carries out the relevant function of macrophage recruitment, as previously suggested (Zhang et al., 2016). Relevant to this point, the deletion of *Smad4* in SMCs of mice with CCR2 deficiency provoked a milder progression of aortic aneurysm with a significantly reduced diameter both in the ascending and in the abdominal tracts of the aorta, thus unravelling a crucial role of CCL2-induced migration of Ly6C^{high} pro-inflammatory monocytes in the aortic pathology of *Smad4^{fl/fl};Myh11-creERT2* mice treated with tamoxifen. Once recruited into the adventitia, the inflammatory infiltrate of monocytes and macrophages progressively spreads into the media and consequently disrupts this layer's structure and aneurysm enlargement and rupture. In addition, an increased number of Ly6C^{low}F4/80^{high} monocytes and macrophages have been detected in the aorta. The function of this cell population was not addressed in this study, but their presence could represent a tissue-reparative response to counterbalance the pro-inflammatory burden.

Although the axis dependent on IL-1 β and CCL2 is key to aneurysm development, we detected modifications of aortic mechanical properties before any sign of inflammatory cell infiltration into the vessel wall, indicating that an early contribution to dilation could come from changes of the composition or structural organization of the media, possibly derived from the observed downregulation of genes such as *Eln*, *Col1a1*, *Lox*, *Itga2*, *Pxn*, and *Vcl*. Our results suggest that IL-1 β is key not only for inflammation but also for regulation of the genes involved in ECM stabilization and cell adhesion.

Abnormal modulation of signaling pathways has been reported in different aneurysm models (Aoki et al., 2007; Gillis et al., 2013). Among the various analyzed, we obtained evidence of NF- κ B activation, specifically a substantial increase in phosphorylation of the RelA subunit. Considering the cross-talk between IL-1 β and NF- κ B, it was relevant to determine which component could activate the other. By analyzing aortas at a time after *Smad4* inactivation when IL-1 β expression was increased only in SMCs and not in fibroblasts or hematopoietic cells, we found that the increase in RelA phosphorylation was abolished in mice with the *Il1r1*-null background. This result

abdominal) and the experimental model used (Alexander et al., 2012; Deguchi et al., 2009; Longo et al., 2002; Martín-Alonso et al., 2015; Shen et al., 2015). In the present context, the orchestration of the activity of proteases from different cellular sources could determine early breaks of elastic lamellae of the media and, later on, the systematic attack of adventitial inflammatory infiltrates from the outer media inward.

In summary, given the SMC-specific recombination in adult animals, we could hypothesize the initial steps of aneurysm development induced by *Smad4* inactivation as follows: (1) loss of *Smad4* function induces IL-1 β expression and activation in SMCs; (2) modulation of *CCL2* expression stimulates monocyte recruitment and inflammation in the adventitia; (3) IL-1 β also activates NF- κ B in SMCs to sustain IL-1 β production, establishing an autocrine mechanism further stimulating the recruitment of innate immune response; (4) in parallel, IL-1 β modifies the expression of specific SMC genes relevant for ECM composition or metabolism and cell adhesion, thus altering the mechanical properties of the arterial wall and vessel diameter; and (5) all these factors contribute to the development of the aortic aneurysm.

The above pathogenetic scheme highlights the central role of IL-1 β in aneurysmal pathology induced by dysregulated TGF- β canonical signaling and indicates this cytokine as an initial target for medical treatment of aneurysms in patients with *SMAD4* mutations.

STAR★METHODS

Detailed methods are provided in the online version of this paper and include the following:

- KEY RESOURCES TABLE
- CONTACT FOR REAGENT AND RESOURCE SHARING
- EXPERIMENTAL MODEL DETAILS
 - Murine Models
- METHODS DETAILS
 - Administration of Neutralizing Anti-IL-1 β Monoclonal Antibody
 - Blood Pressure Measurement
 - Ultrasound Imaging
 - Surgical Procedure and Mounting of Vessels on the Pressure Myograph
 - Murine Primary SMC Cultures
 - Flow Cytometry
 - Histological Analysis
 - Protein Analysis
 - Gene Expression Analysis
- QUANTIFICATION AND STATISTICAL ANALYSIS

SUPPLEMENTAL INFORMATION

Supplemental Information includes seven figures and can be found with this article online at <https://doi.org/10.1016/j.immuni.2017.10.016>.

AUTHOR CONTRIBUTIONS

F.D.R. contributed to gene expression, signaling pathways, and histological, immunocytochemical, and morphometric analyses. R.C. and G.C. performed cardiovascular phenotyping and analyzed data. D.B. helped maintain mouse

colonies. M.C. performed experiments on isolated vessels. M.P. contributed to data analyses and manuscript editing. L.C. analyzed myographic, echographic, and immunofluorescence data. I.V., R.I., and S.F. collected FACS and immunofluorescence data. G.M.B. contributed to the project design and manuscript writing. P.B. handled funding and contributed to work coordination, experiment design, organ dissection, and necroscopic examination. G.L. handled funding and contributed to the project design and manuscript writing. D.C. contributed to the project design, supervised experiments and data and statistical analyses, and drafted the manuscript.

ACKNOWLEDGMENTS

The authors thank Dr. Stefan Offermanns for supplying the Myh11-CreERT2 mice and Novartis for providing the IL-1 β -neutralizing antibody. This work was supported by Ricerca Corrente of the Italian Ministry of Health (to G.L.) and the University of Padova (grant 60A06-8034/14 to P.B.).

Received: February 23, 2017

Revised: July 18, 2017

Accepted: October 26, 2017

Published: November 14, 2017

REFERENCES

- Alexander, M.R., Moehle, C.W., Johnson, J.L., Yang, Z., Lee, J.K., Jackson, C.L., and Owens, G.K. (2012). Genetic inactivation of IL-1 signaling enhances atherosclerotic plaque instability and reduces outward vessel remodeling in advanced atherosclerosis in mice. *J. Clin. Invest.* *122*, 70–79.
- Amento, E.P., Ehsani, N., Palmer, H., and Libby, P. (1991). Cytokines and growth factors positively and negatively regulate interstitial collagen gene expression in human vascular smooth muscle cells. *Arterioscler. Thromb.* *11*, 1223–1230.
- Andrabi, S., Bekheirnia, M.R., Robbins-Furman, P., Lewis, R.A., Prior, T.W., and Potocki, L. (2011). SMAD4 mutation segregating in a family with juvenile polyposis, aortopathy, and mitral valve dysfunction. *Am. J. Med. Genet. A.* *155A*, 1165–1169.
- Aoki, T., Kataoka, H., Shimamura, M., Nakagami, H., Wakayama, K., Moriwaki, T., Ishibashi, R., Nozaki, K., Morishita, R., and Hashimoto, N. (2007). NF-kappaB is a key mediator of cerebral aneurysm formation. *Circulation* *116*, 2830–2840.
- Aoki, T., Kataoka, H., Ishibashi, R., Nozaki, K., Morishita, R., and Hashimoto, N. (2009). Reduced collagen biosynthesis is the hallmark of cerebral aneurysm: contribution of interleukin-1beta and nuclear factor-kappaB. *Arterioscler. Thromb. Vasc. Biol.* *29*, 1080–1086.
- Bardeesy, N., Cheng, K.H., Berger, J.H., Chu, G.C., Pahler, J., Olson, P., Hezel, A.F., Horner, J., Lauwers, G.Y., Hanahan, D., and DePinho, R.A. (2006). *Smad4* is dispensable for normal pancreas development yet critical in progression and tumor biology of pancreas cancer. *Genes Dev.* *20*, 3130–3146.
- Bertoli-Avella, A.M., Gillis, E., Morisaki, H., Verhagen, J.M.A., de Graaf, B.M., van de Beek, G., Gallo, E., Kruihof, B.P.T., Venselaar, H., Myers, L.A., et al. (2015). Mutations in a TGF- β ligand, TGFB3, cause syndromic aortic aneurysms and dissections. *J. Am. Coll. Cardiol.* *65*, 1324–1336.
- Carnevale, D., Cifelli, G., Mascio, G., Madonna, M., Sbroglio, M., Perrino, C., Persico, M.G., Frati, G., and Lembo, G. (2011). Placental growth factor regulates cardiac inflammation through the tissue inhibitor of metalloproteinases-3/tumor necrosis factor- α -converting enzyme axis: crucial role for adaptive cardiac remodeling during cardiac pressure overload. *Circulation* *124*, 1337–1350.
- Carnevale, D., Pallante, F., Fardella, V., Fardella, S., Iacobucci, R., Federici, M., Cifelli, G., De Lucia, M., and Lembo, G. (2014). The angiogenic factor PIGF mediates a neuroimmune interaction in the spleen to allow the onset of hypertension. *Immunity* *41*, 737–752.
- Carnevale, D., Perrotta, M., Pallante, F., Fardella, V., Iacobucci, R., Fardella, S., Carnevale, L., Carnevale, R., De Lucia, M., Cifelli, G., and Lembo, G. (2016). A cholinergic-sympathetic pathway primes immunity in hypertension and mediates brain-to-spleen communication. *Nat. Commun.* *7*, 13035.

- Daugherty, A., and Powell, J.T. (2014). Recent highlights of ATVB: aneurysms. *Arterioscler. Thromb. Vasc. Biol.* *34*, 691–694.
- Davis, F.M., Rateri, D.L., and Daugherty, A. (2014). Mechanisms of aortic aneurysm formation: translating preclinical studies into clinical therapies. *Heart* *100*, 1498–1505.
- Deguchi, J.O., Huang, H., Libby, P., Aikawa, E., Whittaker, P., Sylvan, J., Lee, R.T., and Aikawa, M. (2009). Genetically engineered resistance for MMP collagenases promotes abdominal aortic aneurysm formation in mice infused with angiotensin II. *Lab. Invest.* *89*, 315–326.
- Denes, A., Drake, C., Stordy, J., Chamberlain, J., McColl, B.W., Gram, H., Crossman, D., Francis, S., Allan, S.M., and Rothwell, N.J. (2012). Interleukin-1 mediates neuroinflammatory changes associated with diet-induced atherosclerosis. *J. Am. Heart Assoc.* *1*, e002006.
- Garlanda, C., Dinarello, C.A., and Mantovani, A. (2013). The interleukin-1 family: back to the future. *Immunity* *39*, 1003–1018.
- Gillis, E., Van Laer, L., and Loeys, B.L. (2013). Genetics of thoracic aortic aneurysm: at the crossroad of transforming growth factor- β signaling and vascular smooth muscle cell contractility. *Circ. Res.* *113*, 327–340.
- Guo, X., and Chen, S.Y. (2012). Transforming growth factor- β and smooth muscle differentiation. *World J. Biol. Chem.* *3*, 41–52.
- Guo, D., Hasham, S., Kuang, S.Q., Vaughan, C.J., Boerwinkle, E., Chen, H., Abuelo, D., Dietz, H.C., Basson, C.T., Shete, S.S., and Milewicz, D.M. (2001). Familial thoracic aortic aneurysms and dissections: genetic heterogeneity with a major locus mapping to 5q13–14. *Circulation* *103*, 2461–2468.
- Hayden, M.S., and Ghosh, S. (2012). NF- κ B, the first quarter-century: remarkable progress and outstanding questions. *Genes Dev.* *26*, 203–234.
- He, C.M., and Roach, M.R. (1994). The composition and mechanical properties of abdominal aortic aneurysms. *J. Vasc. Surg.* *20*, 6–13.
- Heald, B., Rigelsky, C., Moran, R., LaGuardia, L., O'Malley, M., Burke, C.A., and Zahka, K. (2015). Prevalence of thoracic aortopathy in patients with juvenile Polyposis Syndrome-Hereditary Hemorrhagic Telangiectasia due to SMAD4. *Am. J. Med. Genet. A.* *167A*, 1758–1762.
- Hiscott, J., Marois, J., Garoufalos, J., D'Addario, M., Roulston, A., Kwan, I., Pepin, N., Lacoste, J., Nguyen, H., Bensi, G., et al. (1993). Characterization of a functional NF- κ B site in the human interleukin 1 beta promoter: evidence for a positive autoregulatory loop. *Mol. Cell. Biol.* *13*, 6231–6240.
- Holm, T.M., Habashi, J.P., Doyle, J.J., Bedja, D., Chen, Y., van Erp, C., Lindsay, M.E., Kim, D., Schoenhoff, F., Cohn, R.D., et al. (2011). Noncanonical TGF β signaling contributes to aortic aneurysm progression in Marfan syndrome mice. *Science* *332*, 358–361.
- Jagadeham, V.P., Scott, D.J., and Carding, S.R. (2008). Abdominal aortic aneurysms: an autoimmune disease? *Trends Mol. Med.* *14*, 522–529.
- Johnston, W.F., Salmon, M., Su, G., Lu, G., Stone, M.L., Zhao, Y., Owens, G.K., Upchurch, G.R., Jr., and Ailawadi, G. (2013). Genetic and pharmacologic disruption of interleukin-1 β signaling inhibits experimental aortic aneurysm formation. *Arterioscler. Thromb. Vasc. Biol.* *33*, 294–304.
- Johnston, W.F., Salmon, M., Pope, N.H., Meher, A., Su, G., Stone, M.L., Lu, G., Owens, G.K., Upchurch, G.R., Jr., and Ailawadi, G. (2014). Inhibition of interleukin-1 β decreases aneurysm formation and progression in a novel model of thoracic aortic aneurysms. *Circulation* *130* (11, Suppl 1), S51–S59.
- Laurent, S., Cockcroft, J., Van Bortel, L., Boutouyrie, P., Giannattasio, C., Hayoz, D., Pannier, B., Vlachopoulos, C., Wilkinson, I., and Struijker-Boudier, H.; European Network for Non-invasive Investigation of Large Arteries (2006). Expert consensus document on arterial stiffness: methodological issues and clinical applications. *Eur. Heart J.* *27*, 2588–2605.
- Lindsay, M.E., and Dietz, H.C. (2011). Lessons on the pathogenesis of aneurysm from heritable conditions. *Nature* *473*, 308–316.
- Lindsay, M.E., Schepers, D., Bolar, N.A., Doyle, J.J., Gallo, E., Fert-Bober, J., Kempers, M.J., Fishman, E.K., Chen, Y., Myers, L., et al. (2012). Loss-of-function mutations in TGFB2 cause a syndromic presentation of thoracic aortic aneurysm. *Nat. Genet.* *44*, 922–927.
- Longo, G.M., Xiong, W., Greiner, T.C., Zhao, Y., Fiotti, N., and Baxter, B.T. (2002). Matrix metalloproteinases 2 and 9 work in concert to produce aortic aneurysms. *J. Clin. Invest.* *110*, 625–632.
- Martín-Alonso, M., García-Redondo, A.B., Guo, D., Camafeita, E., Martínez, F., Alfranca, A., Méndez-Barbero, N., Pollán, Á., Sánchez-Camacho, C., Denhardt, D.T., et al. (2015). Deficiency of MMP17/MT4-MMP proteolytic activity predisposes to aortic aneurysm in mice. *Circ. Res.* *117*, e13–e26.
- Milewicz, D.M., Guo, D.C., Tran-Fadulu, V., Lafont, A.L., Papke, C.L., Inamoto, S., Kwartler, C.S., and Pannu, H. (2008). Genetic basis of thoracic aortic aneurysms and dissections: focus on smooth muscle cell contractile dysfunction. *Annu. Rev. Genomics Hum. Genet.* *9*, 283–302.
- Moriwaki, T., Takagi, Y., Sadamasa, N., Aoki, T., Nozaki, K., and Hashimoto, N. (2006). Impaired progression of cerebral aneurysms in interleukin-1beta-deficient mice. *Stroke* *37*, 900–905.
- Mu, Y., Gudey, S.K., and Landström, M. (2012). Non-Smad signaling pathways. *Cell Tissue Res.* *347*, 11–20.
- Raaz, U., Zöllner, A.M., Schellinger, I.N., Toh, R., Nakagami, F., Brandt, M., Emrich, F.C., Kayama, Y., Eken, S., Adam, M., et al. (2015). Segmental aortic stiffening contributes to experimental abdominal aortic aneurysm development. *Circulation* *131*, 1783–1795.
- Ridker, P.M., Everett, B.M., Thuren, T., MacFadyen, J.G., Chang, W.H., Ballantyne, C., Fonseca, F., Nicolau, J., Koenig, W., Anker, S.D., et al.; CANTOS Trial Group (2017). Antiinflammatory Therapy with Canakinumab for Atherosclerotic Disease. *N. Engl. J. Med.* *377*, 1119–1131.
- Sager, H.B., Heidt, T., Hulsmans, M., Dutta, P., Courties, G., Sebas, M., Wojtkiewicz, G.R., Tricot, B., Iwamoto, Y., Sun, Y., et al. (2015). Targeting Interleukin-1 β Reduces Leukocyte Production After Acute Myocardial Infarction. *Circulation* *132*, 1880–1890.
- Schroder, K., and Tschopp, J. (2010). The inflammasomes. *Cell* *140*, 821–832.
- Shen, M., Lee, J., Basu, R., Sakamuri, S.S., Wang, X., Fan, D., and Kassiri, Z. (2015). Divergent roles of matrix metalloproteinase 2 in pathogenesis of thoracic aortic aneurysm. *Arterioscler. Thromb. Vasc. Biol.* *35*, 888–898.
- Shi, Y., and Massagué, J. (2003). Mechanisms of TGF-beta signaling from cell membrane to the nucleus. *Cell* *113*, 685–700.
- Teekakirikul, P., Milewicz, D.M., Miller, D.T., Lacro, R.V., Regalado, E.S., Rosales, A.M., Ryan, D.P., Toler, T.L., and Lin, A.E. (2013). Thoracic aortic disease in two patients with juvenile polyposis syndrome and SMAD4 mutations. *Am. J. Med. Genet. A.* *161A*, 185–191.
- Trask, A.J., Delbin, M.A., Katz, P.S., Zanesco, A., and Lucchesi, P.A. (2012). Differential coronary resistance microvessel remodeling between type 1 and type 2 diabetic mice: impact of exercise training. *Vascul. Pharmacol.* *57*, 187–193.
- Uçar, A., Öz, F., Baş, F., Ofiaz, H., Nişli, K., Tuğrul, M., Yetim, A., Darendeliler, F., Saka, N., Poyrazoğlu, Ş., and Bundak, R. (2015). Increased arterial stiffness in young normotensive patients with Turner syndrome: associations with vascular biomarkers. *Clin. Endocrinol. (Oxf.)* *82*, 719–727.
- van de Laar, I.M., Oldenburg, R.A., Pals, G., Roos-Hesselink, J.W., de Graaf, B.M., Verhagen, J.M., Hoedemaekers, Y.M., Willemsen, R., Severijnen, L.A., Venselaar, H., et al. (2011). Mutations in SMAD3 cause a syndromic form of aortic aneurysms and dissections with early-onset osteoarthritis. *Nat. Genet.* *43*, 121–126.
- Weber, A., Wasiliew, P., and Kracht, M. (2010). Interleukin-1 (IL-1) pathway. *Sci. Signal.* *3*, cm1.
- Wirth, A., Benyó, Z., Lukasova, M., Leutgeb, B., Wettchschureck, N., Gorbey, S., Orsy, P., Horváth, B., Maser-Gluth, C., Greiner, E., et al. (2008). G12-G13-LARG-mediated signaling in vascular smooth muscle is required for salt-induced hypertension. *Nat. Med.* *14*, 64–68.
- Yang, P., Schmit, B.M., Fu, C., DeSart, K., Oh, S.P., Berceli, S.A., and Jiang, Z. (2016). Smooth muscle cell-specific Tgfr1 deficiency promotes aortic aneurysm formation by stimulating multiple signaling events. *Sci. Rep.* *6*, 35444.
- Zacchigna, L., Vecchione, C., Notte, A., Cordenonsi, M., Dupont, S., Maretto, S., Cifelli, G., Ferrari, A., Maffei, A., Fabbro, C., et al. (2006). Emilin1 links TGF-beta maturation to blood pressure homeostasis. *Cell* *124*, 929–942.
- Zhang, P., Hou, S., Chen, J., Zhang, J., Lin, F., Ju, R., Cheng, X., Ma, X., Song, Y., Zhang, Y., et al. (2016). Smad4 Deficiency in Smooth Muscle Cells Initiates the Formation of Aortic Aneurysm. *Circ. Res.* *118*, 388–399.

STAR★METHODS

KEY RESOURCES TABLE

REAGENT or RESOURCE	SOURCE	IDENTIFIER
Antibodies		
Mouse anti- α -SMA for immunohistochemistry or immunofluorescence	Sigma Aldrich	A5228; RRID: AB_262054
Rabbit anti-Collagen I for immunohistochemistry or immunofluorescence	Acris	R1038; RRID: AB_978381
Rabbit anti-IL1 beta for immunohistochemistry or immunofluorescence	Genetex	GTX74034; RRID: AB_378141
Rabbit anti-IL1 Receptor I for immunohistochemistry or immunofluorescence	Abcam	ab106278; RRID: AB_10865509
Rabbit anti-Smad4 for immunohistochemistry or immunofluorescence	Santa Cruz	sc-7154; RRID: AB_2302322
Rat anti-CD11b for immunohistochemistry or immunofluorescence	Abd Serotec	MCA711G; RRID: AB_323167
Rat anti-CD3 for immunohistochemistry or immunofluorescence	eBioscience	17-0032; RRID: AB_10597589
Rat anti-CD45 for immunohistochemistry or immunofluorescence	Abd Serotec	MCA 1388; RRID: AB_321729
Rat anti-CD68 for immunohistochemistry or immunofluorescence	Abd Serotec	MCA 1957GA; RRID: AB_324217
Rat anti-ER-TR7 for immunohistochemistry or immunofluorescence	Santa Cruz	sc-73355; RRID: AB_1122890
Goat anti-Myh11 for western blot	Santa Cruz	sc-79079; RRID: AB_3231672147150
Mouse anti-Smad4 for western blot	Santa Cruz	sc-7966; RRID: AB_2184015
Mouse anti- β -actin for western blot	Sigma Aldrich	A5316; RRID: AB_476743
Rabbit anti P-ERK 1/2 for western blot	Santa Cruz	sc-101760; RRID: AB_2139987
Rabbit anti P-TAK1 for western blot	Cell Signaling	4531; RRID: AB_390772
Rabbit anti-MLC20 for western blot	Santa Cruz	sc-376606; RRID: AB_11150665
Rabbit anti-P-(S536) RelA/p65 for western blot	Cell Signaling	3033; RRID: AB_331284
Rabbit anti-P-JNK for western blot	Cell Signaling	9251; RRID: AB_331659
Rabbit anti-P-MLC20 for western blot	Cell Signaling	3671P; RRID: AB_330248
Rabbit anti-P-MYPT1 for western blot	Santa Cruz	sc-17556; RRID: AB_653348
Rabbit anti-P-p38 for western blot	Cell Signaling	9215; RRID: AB_331762
Rabbit anti-P-Smad1/5/8 for western blot	Merck Millipore	AB3848; RRID: AB_177439
Rabbit anti-P-Smad2 for western blot	Cell Signaling	3101; RRID: AB_331673
Rabbit anti-RelA/p65 for western blot	Santa Cruz	sc-372; RRID: AB_632037
Rabbit anti-TAK1 for western blot	Bethyl	A301-915A; RRID: AB_1524082
Alexa488 anti-mouse, secondary antibody	Jackson ImmunoResearch	715-545-150; RRID: AB_2340846
Cy3 anti-rabbit, secondary antibody	Jackson ImmunoResearch	111-165-003; RRID: AB_2338000
Cy3 anti-rat, secondary antibody	Jackson ImmunoResearch	112-165-167; RRID: AB_2338251
HRP anti-mouse, secondary antibody	Bethyl	A90-116P; RRID: AB_67183
HRP anti-rabbit, secondary antibody	Bethyl	A120-101P; RRID: AB_67264
BUV395 CD45 (clone 30-F11) for flow cytometry	BD Horizon	564279; RRID: AB_2651134
BUV737 CD11b (clone M1/70) for flow cytometry	BD Horizon	564443
BV421-Ly6C (clone AL-21) for flow cytometry	BD Horizon	562727
BV510-F4/80 (clone BM8) for flow cytometry	Biolegend	123135; RRID: AB_2562622
BV605-CD29 (clone HM β 1-1) for flow cytometry	BD OptiBuild	740365
BV711-CD31 (clone MEC 13.3) for flow cytometry	BD OptiBuild	740680

(Continued on next page)

Continued

REAGENT or RESOURCE	SOURCE	IDENTIFIER
CD16/CD32 (clone 2.4G2) for flow cytometry	BD PharMingen	553141; RRID: AB_394656
FITC- α SMA (clone 1A4) for flow cytometry	Abcam	ab8211; RRID: AB_306359
PE CD19 (clone 1D3) for flow cytometry	BD PharMingen	553786; RRID: AB_395050
PE CD45R/B220 (cloneRA3-6B2) for flow cytometry	BD PharMingen	553090; RRID: AB_394620
PE CD49b (clone DX5) for flow cytometry	BD PharMingen	553858; RRID: AB_395094
PE CD90.2 (clone 53-2.1) for flow cytometry	BD PharMingen	553006; RRID: AB_394545
PE IgG2B (clone 141945) for flow cytometry	R&D Systems	IC013P; RRID: AB_357259
PE IL-1 β (clone 166931) for flow cytometry	R&D Systems	IC4013P; RRID: AB_10719123
PE Ly6G (clone 1A8) for flow cytometry	BD PharMingen	551461; RRID: AB_394208
PE NK1.1 (clone PK136) for flow cytometry	BD PharMingen	553165; RRID: AB_394677
PE Ter-119 (clone TER-119) for flow cytometry	BD PharMingen	553673; RRID: AB_394986
<i>In vivo</i> mouse anti-mouse IL-1 β IgG2a/k	Novartis	N/A
<i>In vivo</i> mouse IgG2a isotype control (C1.18.4)	BioXCell	BP0085; RRID: AB_1107771
Chemicals, Peptides, and Recombinant Proteins		
7-AAD	BD PharMingen	559925
Alcian Blue 8GX	Sigma Aldrich	A5268
Collagenase type I	Worthington	CLS-1
Collagenase type I	Sigma Aldrich	C0130
Collagenase type XI	Sigma Aldrich	C7657
Corn Oil	Sigma Aldrich	C8267
DAPI Vectashield	Vector Laboratories	H-1500
Eosin Y	Sigma Aldrich	230251
Hematoxylin	Invitrogen	51275
Hoechst 33258	Sigma Aldrich	861405
Hoechst 33342	Invitrogen	C10338
Hyaluronidase	Sigma Aldrich	H3506
IL-1 β peptide	Immunotools	12340013
LiteAblot EXTEND	Euroclone	EMP013001
LiteAblot PLUS	Euroclone	EMP011005
Lypopolisaccharide (Salmonella Enterica)	Sigma Aldrich	L5886
Non-fat dry milk	Biorad	170-6404
NuPAGE 10% Bis-Tris Gel	Novex	NP0301BOX
NuPAGE LDS Sample Buffer	Novex	NP0007
NuPAGE Sample Reducing Agent	Novex	NP0009
SB525334	Sigma Aldrich	060916
Tamoxifen	Sigma Aldrich	T5648
TBS-0.1% Tween20 buffer	Sigma Aldrich	P7949
TGF- β peptide	R&D Systems	7666-MB
Total extraction Kit	Merck Millipore	2140
Trizol	Invitrogen	15596018
Critical Commercial Assays		
Anti-rabbit ELITE VectaStain Kit	Vector Laboratories	PK-6101; RRID: AB_2336820
cOmplete, EDTA-free	Roche	11873580001
Fixation/Permeabilization Kit with GolgiPlug	BD Cytotfix/Cytoperm Plus	555028
PhosSTOP EASYpack	Roche	04906837001
Pierce BCA Protein Assay Kit	Thermo Scientific	23227
Experimental Models: Organisms/Strains		
Mouse: <i>Smad4</i> ^{fl/fl}	Dr. DePinho (Boston)	N/A
Mouse: <i>Myh11-creERT2</i>	Dr. Offermanns (Heidelberg)	N/A

(Continued on next page)

Continued

REAGENT or RESOURCE	SOURCE	IDENTIFIER
Mouse: <i>Il1r1^{tm1/mx}</i>	The Jackson Laboratory	028398; RRID: IMSR_JAX:02839
Mouse: <i>Ccr2^{tm1/fc}</i>	The Jackson Laboratory	004999; RRID: IMSR_JAX:004999
Mouse: C57BL/6Ncr1	Charles River	N/A
Oligonucleotides		
<i>Eln</i> , primers GCTGTGTCACCAGCTGCAG (forward) and CTCCAAGTCTGCTCCAGC (reverse)	N/A	N/A
<i>Fn1</i> , primers CTGTCAACCTCTGCAGACCTA (forward) and TTCCTTCCAGCGACCCGTAG (reverse)	N/A	N/A
<i>Col1a1</i> , primers GAGCGGAGAGTACTGGATCG (forward) and GCTTCTTTTCTTGGGGTTC (reverse)	N/A	N/A
<i>Col3a1</i> , primers TCCCATTGGAGAATGTTGTGCAAT (forward) and CCAGGAGGCCAGGGAGA (reverse)	N/A	N/A
<i>Tnc</i> , primers TTCGTGTGTTGCCATCTTGGGA (forward) and ATGATCTCCCATGTTTCGAAAGCA (reverse)	N/A	N/A
<i>Thbs1</i> , primers GAACCTCCAAAATGACCCTAA (forward) and TACAGACAGGCCTGAGTATCC (reverse)	N/A	N/A
<i>Lox</i> , primers CTGCGGAAGAAAAGTGCCTG (forward) and CGTAGCAGTACCCTGTGGTC (reverse)	N/A	N/A
<i>Itga1</i> , primers CAATGCCTTGTGTGAAGTTGGA (forward) and GAAATCCTCCCTTCGGATTGGTG (reverse)	N/A	N/A
<i>Itga2</i> , primers ATATTCAGCATTGAAGGCAC (forward) and GGCTTGTTTAGGAAAGATCAC (reverse)	N/A	N/A
<i>Itga5</i> , primers GAACACAAGTTCTGAAATGC (forward) and ATATACAGCCTCACACTGAAG (reverse)	N/A	N/A
<i>ItgaV</i> , primers GACAGTTATTTGGGTTACTCTG (forward) and GAAAATCCAAAATACGCAGC (reverse)	N/A	N/A
<i>Itgb1</i> , primers CCTACAACCTCTTTCTTCAG (forward) and CTTTCGTCCATTTTCTCCTG (reverse)	N/A	N/A
<i>Itgb3</i> , primers TATAGTGAGCTCATTCTCTGG (forward) and ATTTTCCCGTAAGCATCAAC (reverse)	N/A	N/A
<i>Csrp1</i> , primers CCCTGCTACTCCGCCATGTTT (forward) and TACTTGAAAAGTGTGGCTCTCAGC (reverse)	N/A	N/A
<i>Csrp2</i> , primers GTCCTCGATGCAACAAGAGAGTG (forward) and CCTGGGGTCAGGGTCTTGG (reverse)	N/A	N/A
<i>Csrp3</i> , primers CAGCACAGACACTGGCGAGC (forward) and CACATCGTGGGCACTTCTCTG (reverse)	N/A	N/A
<i>Tgfb1i1</i> , primers GCCTCTGTGGCTCCTGCAATAAA (forward) and CTTCTGAAGAAGCTGCTGCCT (reverse)	N/A	N/A
<i>Fhl1</i> , primers GCCCATAAGCGCTGATGCCAAG (forward) and GGGGTGAAGGCACTTGGCACA (reverse)	N/A	N/A
<i>Fhl2</i> , primers CTCGTCCAAGTGCCAGGAATG (forward) and CTTAGGTATGAAGCTCTTGGTTCC (reverse)	N/A	N/A
<i>Zyx</i> , primers GGCTGCTACACCGACACTTTG (forward) and CTCAGCATGCGGTCAGTGAT (reverse)	N/A	N/A
<i>Trip6</i> , primers GAGGTGGCATGAGCCTCAG (forward) and GGTGGCTCATGTCATGCACCA (reverse)	N/A	N/A
<i>Lpp</i> , primers CCAGTTGTTGCTCCGAAACCC (forward) and GGAGGAGGAGGGAAGTGTG (reverse)	N/A	N/A
<i>Pxn</i> , primers GCTGCCTCAACACCTCAAC (forward) and GCTGCCTCAACACCTCAAC (reverse)	N/A	N/A
<i>Ptk2</i> , primers GCGGACACATGCAGTCTCTG (forward) and TTGCAACAGCCAAAGCTGGATTC (reverse)	N/A	N/A

(Continued on next page)

Continued

REAGENT or RESOURCE	SOURCE	IDENTIFIER
<i>Vcl</i> , primers CTGACCAAGTGGCTGACCTC (forward) and GCTTCCGAGCTGCATTCTCC (reverse)	N/A	N/A
<i>Bcar1</i> , primers CGAGGACTGCTTCCTAACCAG (forward) and GGACGAGAGCAGGCCCTTCT (reverse)	N/A	N/A
<i>Abi1</i> , primers GCCAGTGGAGATAAACTCTCA (forward) and CGTTTGGGCTTCACACCATT (reverse)	N/A	N/A
<i>I11b</i> , primers ACCTGTGTCTTCCCGTGGAC (forward) and GGGAACGTCACACACCAGCA (reverse)	N/A	N/A
<i>Nlrp3</i> , primers GGAGAAGGCAGATCATTGG (forward) and CAGCAAACCATCCACTCTT (reverse)	N/A	N/A
<i>I16</i> , primers AACTCCTTAGTCCTCGGCCA (forward) and CACGATTCCCAGAGAATGTG (reverse)	N/A	N/A
<i>I18</i> , primers CGAGGATATGACTGATATTGATCAAAG (forward) and ACTATCCTTCACAGAGAGGGTCA (reverse)	N/A	N/A
<i>I14</i> , primers CACGGATGCGACAAAATCA (forward) and CGTTGCTGTGAGGACGTTTG (reverse)	N/A	N/A
<i>I10</i> , primers ATGCTGCCTGCTCTTACTGACTG (forward) and CCCAAGTAACCCTTAAAGTCCTGC (reverse)	N/A	N/A
<i>Ccl2</i> , primers CTTCTGGCCTGCTGTTCA (forward) and CCAGCCTACTCATTGGGATCA (reverse)	N/A	N/A
<i>Cxcl10</i> , primers ATGACGGGCCAGTGAGAATG (forward) and TCAACACGTGGGCAGGATAG (reverse)	N/A	N/A
<i>Cxcl12</i> , primers CATTGACCCGAAATTA (forward) and CTCTTCTTCTGTCGCTTCT (reverse)	N/A	N/A
<i>Ccl5</i> , primers GCAGTCGTGTTTGTCACTCG (forward) and AGAGCAAGCAATGACAGGGA (reverse)	N/A	N/A
<i>Tnf</i> , primers GGCCTCCCTCTCATCAGTTC (forward) and GTTGCTTTGAGATCCATGCCG (reverse)	N/A	N/A
<i>Ifng</i> , primers AGAGCCAGATTATCTCTTTCTACCTCAG (forward) and CCTTTTTCGCCTTGCTGTTG (reverse)	N/A	N/A
<i>Ifnb</i> , primers GGAGATGACGGAGAAGATGC (forward) and CCCAGTGCTGGAGAAATTGT (reverse)	N/A	N/A
<i>Mmp1</i> , primers GTCTTTGAGGAGGAAGGCGA (forward) and CAAACCTAGGCCTGGCAGAA (reverse)	N/A	N/A
<i>Mmp2</i> , primers TGGAATGCCATCCCTGATAA (forward) and AGCCCAGCCAGTCTGATTG (reverse)	N/A	N/A
<i>Mmp8</i> , primers ATCCTTGCCCATGCCTTTCAA (forward) and CCAAATTCATGAGCAGCCAC (reverse)	N/A	N/A
<i>Mmp9</i> , primers TTGAAGTCTCAGAAGGTGGAT (forward) and GCAGGAGTCTGTAGGTCAC (reverse)	N/A	N/A
<i>Mmp12</i> , primers AAAGTGGGTTGTAGCATTGC (forward) and AGAAGGCAGACCAGGACAC (reverse)	N/A	N/A
<i>Mmp13</i> , primers GGTCTTCTGGCACAGCTTT (forward) and CAAGCTCATGGCAGCAACA (reverse)	N/A	N/A
<i>Ctss</i> , primers ATAAAGGCTGTGGAGGCG (forward) and CATCCGTGGCTTTGTAGG (reverse)	N/A	N/A
<i>Tgfb1</i> , primers TTGCTTCAGCTCCACAGAGA (forward) and TGGTTGTAGAGGGCAAGGAC (reverse)	N/A	N/A
<i>Tgfb2</i> , primers CAGCGCTACATCGATAGCAA (forward) and CCTCGAGCTCTTCGCTTTTA (reverse)	N/A	N/A
<i>Tgfb3</i> , primers GATGAGCACATAGCCAAGCA (forward) and ATTGGGCTGAAAGGTGTGAC (reverse)	N/A	N/A
<i>Tgfb1</i> , primers CCTGGGATTTATAGCAGCAGAC (forward) and CAGTAACAGTGATCTATTCAAGTA (reverse)	N/A	N/A

(Continued on next page)

Continued

REAGENT or RESOURCE	SOURCE	IDENTIFIER
<i>Tgfb2</i> , primers GAGAAGCCGCATGAAGTCTG (forward) and GACACACTTGGGAGAAGCGG (reverse)	N/A	N/A
<i>Smad2</i> , primers CCAGCAGGAATTGAGCCACA (forward) and CTGTGTCCATACTTTGGTTCAAC (reverse)	N/A	N/A
<i>Smad3</i> , primers GAACACTAATTCCCTGTGG (forward) and CTGCGTCCATGCTGTGGTTC (reverse)	N/A	N/A
<i>Smad4</i> , primers GAGCTTGCATTCCAGCCTCC (forward) and CACAACAGGGCAGCTTGAAGG (reverse)	N/A	N/A
<i>Bmp2</i> , primers CAGCCGCGCCAACACCGT (forward) and CAGATGTGAGAACTCGTCACTG (reverse)	N/A	N/A
<i>Bmp4</i> , primers CGTCCCGCCAGCCGAGC (forward) and GCCGAGGAGATCACCTCATTG (reverse)	N/A	N/A
<i>Bmp6</i> , primers CTCCAGCTGAGTGTGGTGACT (forward) and GGACCTCGCTCACCTTGAAGA (reverse)	N/A	N/A
<i>Alk2</i> , primers CATCACGGCCAGCTGCC (forward) and CCACCGAGAGGATGATAAGGC (reverse)	N/A	N/A
<i>Alk3</i> , primers GCCCAGATGATGCTATTAATAACAC (forward) and CAGAGCCTTCATACTTCATACACC (reverse)	N/A	N/A
<i>Alk6</i> , primers CCACTCTGCCTCCTCTCAAG (forward) and CCAAGAGTAACTACAGACAGTCA (reverse)	N/A	N/A
<i>Bmpr2</i> , primers CCTGGATAACCTGAAGCTGCTG (forward) and CAGCAACTGGACGCTCATCCAA (reverse)	N/A	N/A
<i>Acvr2a</i> , primers CTGGCAAGTCTGCAGGTGAC (forward) and TATCTATCCTCAGAAATGCGTCCC (reverse)	N/A	N/A
<i>Acvr2b</i> , primers GTGGCTGTGAAGATCTTCCCAC (forward) and GGCAGCAATGAACTGCAACAAGTT (reverse)	N/A	N/A
<i>Pai1</i> , primers ATGGAGCCTTGACAGTGGG (forward) and GAGGTCTGGGATGCTGGTT (reverse)	N/A	N/A
<i>Ctgf</i> , primers TCCACCCGAGTTACCAATG (forward) and TAGCCCTGTATGTCTTCACAC (reverse)	N/A	N/A
<i>Id1</i> , primers CTGCAGCATGTAATCGACTAC (forward) and TCGTCCGGCTGGAACACATG (reverse)	N/A	N/A
<i>Id2</i> , primers AAAACAGCCTGTCCGACCAC (forward) and CTGGGCACCAGTTCCTTGAG (reverse)	N/A	N/A
<i>Id3</i> , primers AGCTTAGCCAGGTGGAATCCT (forward) and TCAGCTTGTCTGGATCGGGAG (reverse)	N/A	N/A
<i>Acta2</i> , primers GAGAAGCCCAGCCAGTTCG (forward) and CTCTTGCTCTGGGCTTCATC (reverse)	N/A	N/A
<i>Myh11</i> , primers CCCAACCCACTCCCAACCT (forward) and TGCTCTGCTCCGCTCGCTC (reverse)	N/A	N/A
<i>Sm22</i> , primers TCCAGTCCACAACGACCAAG (forward) and GAATTGAGCCACCTGTTCCATCT (reverse)	N/A	N/A
<i>Cnn1</i> , primers CTTCTCGCCAGGTGTACG (forward) and TGTGCGGGTGGTATTGTG (reverse)	N/A	N/A
<i>Smtn</i> , primers CGCACGATTGGCAGGGAGA (forward) and GTCTACTGCACAGTCTCCAG (reverse)	N/A	N/A
Software and Algorithms		
Primer3 Software	N/A	N/A
ImageJ Software	NIH	N/A
GraphPad Software PRISM5	PRISM5	N/A
SPSS 23.0 Software	IBM	N/A
FACSDiva Software	BD Biosciences	N/A
FlowJo V10.0.8 Software	Tree Star	N/A
MyoVIEW II Software	DMT	N/A

CONTACT FOR REAGENT AND RESOURCE SHARING

Further information and requests for resources and reagents should be directed to and will be fulfilled by the Lead Contact, Giuseppe Lembo (giuseppe.lembo@uniroma1.it).

EXPERIMENTAL MODEL DETAILS

Murine Models

All animal handling and experimental procedures were performed according to European Community guidelines (EC Council Directive 2010/63) and the Italian legislation on animal experimentation (Decreto Legislativo D.Lgs 26/2014). All efforts were made to minimize suffering, and the principles of Replacement, Reduction, and Refinement (i.e., the “three Rs”) were applied to all experiments. Mice were housed in an air-conditioned room (temperature $21^{\circ}\text{C} \pm 1^{\circ}\text{C}$, relative humidity $60\% \pm 10\%$), with lights on from 06:00 to 18:00, and had sawdust as bedding, pellet food, and tap water *ad libitum*.

Mouse strains used included *Smad4^{fl/fl}* (Bardeesy et al., 2006), *Myh11-creERT2* (Wirth et al., 2008), *Il1r^{-/-}* (*Il1r^{tm1/mx}*, The Jackson Laboratory), *Ccr2^{-/-}* (*Ccr2^{tm1/fc}*, The Jackson Laboratory). All the mice were backcrossed in the C57BL/6 strain (Charles River Laboratories). As the *Myh11-creERT2* transgene is Y linked and females do not express the Cre recombinase, only male mice were used. Cre-Lox recombination was induced in 8- to 12-week-old male mice by tamoxifen (T5648, Sigma Aldrich) administration at the dose of 166 mg/kg/day in corn oil by oral gavage for 5 consecutive days. Control groups received corn oil on a similar schedule.

METHODS DETAILS

Administration of Neutralizing Anti-IL-1 β Monoclonal Antibody

The IL-1 β neutralizing antibody was a donation from Novartis (Basel, Switzerland). The antibody selectively binds IL-1 β , thus blocking the interaction of the cytokine with its receptors. We treated mice once weekly with a monoclonal mouse anti-mouse IL-1 β IgG2a/k antibody (or a mouse monoclonal IgG2a isotype control), after the last day of tamoxifen or vehicle, with subcutaneous injections of 10 mg/kg body/weight (Denes et al., 2012; Sager et al., 2015).

Blood Pressure Measurement

Blood pressure measurement was performed by tail-cuff plethysmography (BP-2000 Series II, Visitech Systems), as previously described (Carnevale et al., 2014; Zacchigna et al., 2006), with operators blinded to the experimental group.

Ultrasound Imaging

Ultrasonographic analyses were performed with Vevo2100 (Visualsonics, Fujifilm) equipped by 40 MHz transducer. Mice were anesthetized with isoflurane (5% induction and 1.5%–2.0% maintenance). Cardiac function was obtained by standard echocardiography (Carnevale et al., 2011). For vascular analysis, the ultrasound transducer was placed on the right side of upper anterior mediastinum for the ascending aorta (Figure S7A), and on the mouse abdomen for the abdominal aorta (Figure S7B). In order to standardize this projection 3 reference points were used: aortic valve, pulmonary artery, and the brachiocephalic trunk (Figure S7A). B-mode images were acquired using Visual Sonics presets and measurements of aortic diameters were obtained using Anatomical M-mode. For the measurement of maximum vessel diameter, sample volume (SV) was positioned on the ascending aorta in correspondence of the center of the pulmonary artery and perpendicular to vessel wall. In our model, abdominal aneurysms developed only in the suprarenal region of the vessels (Figure S7B). Thus we acquired B-mode images in correspondence to that point and we measured the maximum vessel diameter through Anatomical M-mode, placing the SV perpendicular to vessel wall. *In vivo* mechanical properties were assessed through calculations of the following standard parameters (Laurent et al., 2006 and Uçar et al., 2015, respectively):

$$\text{distensibility coefficient (DC)} = \frac{\Delta A}{A * \Delta p}$$

$$\beta - \text{index} = \frac{\ln\left(\frac{\text{SBP}}{\text{DBP}}\right)}{\frac{\Delta D}{D}}$$

where ΔA = change in lumen area during systole, A = lumen area during diastole, Δp = pulse pressure, SBP = systolic blood pressure, DBP = diastolic blood pressure, ΔD = change in lumen diameter during systole, and D = lumen diameter during diastole.

Surgical Procedure and Mounting of Vessels on the Pressure Myograph

For mechanical studies, vessels were excised from mice after cervical dislocation, cleaned of connective and fat tissues, then cannulated and mounted on a pressure myograph (DMT, Danish Myotechnology). The experiments were performed in physiological buffer at 37°C of the following composition: 135 mM NaCl, 5 mM KCl, 1.6 mM CaCl_2 , 1.17 mM MgSO_4 , 0.44 mM KH_2PO_4 ,

2.6 mM NaHCO₃, 0.34 mM Na₂HPO₄, 5.5 mM D-glucose, 0.025 mM EDTA, 10 mM HEPES (pH 7.4). After 30-minute equilibration, vessels were transilluminated under an inverted microscope connected to a computerized system for continuous recording of measures.

Recordings of vessel inner diameters (IDs) and outer diameters (ODs) were taken while increasing the intravascular (transmural) pressure from 0 to 175 mmHg by steps of 25 mmHg (5 min per step). Recordings were also taken while decreasing the pressure following the same steps and timing from 175 to 0 mmHg. Since the thickness of the wall in the large arteries (like the ascending aorta) precluded the localization of the inner wall edge in many transilluminated vessels at pressures lower than 100–125 mmHg, the ID was obtained as an indirect measure, calculated by estimating that vessel wall cross-sectional area (WCSA) remains constant throughout the experimental pressure range. Thus ID can be accurately calculated from OD at any given pressure and from a single measurement of WCSA. Wall/lumen ratio, cross sectional area, circumferential strain, circumferential wall stress, and incremental elastic modulus were calculated according to the following formulas (Trask et al., 2012):

$$\text{wall/lumen ratio} = \left(\frac{WT}{D_i} \right) * 100$$

$$\text{cross - sectional area (CSA)} = \pi * \frac{D_e^2 - D_i^2}{4}$$

$$\text{circumferential strain } (\epsilon) = \frac{D_i - D_0}{D_0}$$

$$\text{circumferential stress } (\sigma) = \frac{p * D_i}{2 * WT}$$

$$\text{incremental elastic modulus (E)} = \frac{\Delta\sigma}{\Delta\epsilon}$$

where WT = wall thickness, D_e = external diameter, D_i = internal diameter, p = pressure in dynes/cm², and D₀ = original diameter measured at 0 mmHg.

For IL-1β immunolocalization by confocal microscopy, vessels were prepared with the same procedure described above and kept pressurized at 125 mmHg for 6 hr in physiological buffer at 37°C. As required by the protocol, vessels were incubated with the following substances: 10 ng/mL LPS from *Salmonella Enterica* (L5886, Sigma Aldrich), 10 ng/mL recombinant mouse TGF-β (7666-MB, R&D Systems), 10 μM SB525334 (060916, Sigma Aldrich).

Murine Primary SMC Cultures

Arteries were dissected out from wild-type mice and cleaned from surrounding tissues. Arteries were then incubated in 138 U/mL of Collagenase type I (CLS-1, Worthington) in DMEM for 40 min at 37°C. After removing adventitia, the samples were incubated in 0.25% Trypsin-EDTA (Life Technologies) for 6 min at 37°C. The tissue was minced and plated on dishes precoated with 0.1% gelatin in PBS and cultured in DMEM, 20% FBS and penicillin/streptomycin. For the proposed experiments only cells from passage 1 and passage 2 were used.

For mRNA analysis, wild-type SMCs were starved in DMEM, 0.1% FBS, penicillin/streptomycin for 16 hr and then treated with LPS for 6 hr or with 10 ng/mL IL-1β (12340013, Immunotools) for 24 hr, as indicated in figures.

Flow Cytometry

After mice were exsanguinated, aortas were collected and directly analyzed for myeloid staining. For IL-1β analysis, vessels were incubated for 6 hr in the presence of: 10 ng/mL LPS, 10 ng/mL recombinant mouse TGF-β (7666-MB, R&D Systems), 10 μM SB525334 (060916, Sigma Aldrich), as specifically indicated in figures.

Single cell suspensions were obtained as previously described (Carnevale et al., 2014; Carnevale et al., 2016). In brief, aortas were digested with the following cocktail: Collagenase type XI (C7657, Sigma Aldrich), Collagenase type I (C0130, Sigma Aldrich), Hyaluronidase (H3506, Sigma Aldrich), at 700 rpm for 40 min at 37°C. The digested aortas were then passed through a 70 μm sterile filter (Falcon BD Bioscience) and centrifuged at 1500 rpm for 5 min at 4°C. The pellet was resuspended in a buffer containing 0.5% BSA, 0.1% sodium azide and 2 mM EDTA and number of live cells was assessed using trypan blue and an automated counter (Countess, Life Technologies). Anti-CD16/CD32 (2.4G2, BD Bioscience) was added for 10 min at room temperature (RT) for blocking of nonspecific binding and then primary antibodies were incubated for 20 min at RT. After washing, cells were incubated for 10 min with viability marker 7-AAD (BD Bioscience).

For myeloid cell staining, the following primary antibodies were used: lineage markers (PE-CD49b (clone DX5), PE-CD45R/B220 (clone RA3-6B2), PE-CD90.2 (clone 53-2.1), PE-CD19 (clone 1D3), PE-NK1.1 (clone PK136), PE-Ter119 (clone TER 119) PE-Ly6G (clone 1A8) from BD Bioscience), BUV737-CD11b (clone M1/70), BV421-Ly6C (clone AL-21), BUV395-CD45 (clone 30-F11) from BD Bioscience, BV510-F4/80 (clone BM8) from BioLegend. Monocytes were identified as (Lineage)^{low}(CD45 and CD11b)^{high}(F4/80)^{low}(Ly6C)^{high} and macrophages as (Lineage)^{low}(CD45 and CD11b)^{high}(Ly6C)^{low/int}(F4/80)^{high}, as exemplified in the gating strategy showed in [Figure S7C](#).

For IL-1 β staining, the following primary antibodies for surface markers were used: BUV395-CD45 (clone 30-F11), BUV737-CD11b (clone M1/70), BV711-CD31 (clone MEC 13.3), BV605-CD29 (clone HM β 1-1) from BD Bioscience, BV510-F4/80 (clone BM8) from BioLegend. For intracellular markers, antibodies were added after fixing and permeabilization of samples with the fixation/permeabilization kit BD Cytotfix/Cytoperm (BD Bioscience). The primary antibodies for intracellular staining were as follow: FITC- α SMA (clone 1A4, Abcam) and PE-IL-1 β /IL-1F2 (clone 166931, R&D Systems) or its isotype PE-IgG2B (clone 141945, R&D Systems). Cells positive for IL-1 β were analyzed using the fluorescence minus one (FMO) gating on SMCs (CD45⁻CD31⁻ α SMA⁺), fibroblasts (CD45⁻CD31⁻CD29⁺), endothelial cells (CD45⁻CD31⁺), monocytes and macrophages (CD45⁺CD11b⁺), as exemplified in the gating strategy shown in [Figure S7D](#). Data from the entire sample were acquired on FACSCelesta flow cytometer with FACSDiva software (BD Biosciences) and analyzed using FlowJo software (V10.0.8, Tree Star).

Histological Analysis

Hematoxylin & eosin (H&E) and Weigert's staining were carried out on paraformaldehyde-fixed (4% overnight at 4°C) paraffin-embedded or frozen sections (7–10 μ m) using standard procedures. For Alcian Blue staining frozen aorta sections were fixed in 10% paraformaldehyde and stained with 1% solution for 3 hr at RT. For immunoperoxidase staining, the anti-rabbit VectaStain Kit (Vector laboratories) was used following manufacturer's protocol.

For immunofluorescence frozen sections were treated with MetOH/Aceton (1:1) at –20°C for 10' before incubation with blocking solution. Slides were incubated at 4°C overnight with primary antibody and for 2 hr at RT with secondary antibody, mounted, and examined in a Leica SP5 confocal microscope or a Zeiss 780 confocal microscope.

Primary antibodies used for immunofluorescence or immunohistochemistry were: rabbit anti-Smad4 (1:200; Santa Cruz); rat anti-ER-TR7 (1:250; Santa Cruz); mouse anti- α -SMA (1:200; Sigma Aldrich); rat anti-CD45 (1:250; Abd Serotec); rat anti-CD68 (1:250; Abd Serotec); rat anti-CD3 (1:250; eBioscience); rat anti-CD11b (1:250; Abd Serotec); rabbit anti-Collagen I (1:1,600; Acris); rabbit anti-IL-1 β (1:1,000; GeneTex); rabbit anti-IL-1R (1:100; Abcam). Secondary antibodies used were Alexa488 anti-mouse (1:200), Cy3 anti-rat (1:300), Cy3 anti-rabbit (1:200) (all Jackson ImmunoResearch). Nuclei were stained with Hoechst (33258, Sigma Aldrich) or DAPI Vectashield (Vector laboratories) as indicated in figure legends.

IL-1 β staining was quantified by automated fluorescence signal detection analysis and expressed as % of signal intensity in SMCs area of the vessels ([Figures S7E](#) and [S7F](#)). Quantitative analysis of IL-1 β staining was performed by measurement of stained area ([Figure S7E](#)) over global SMCs area of the vessel, labeled with anti- α -SMA ([Figure S7F](#), dashed area) with ImageJ software (NIH). Data are expressed as mean percentage \pm SEM.

Protein Analysis

Proteins were extracted from aortas using the "Total protein extraction kit" (Merck Millipore) as indicated by the manufacturer, supplemented with protease and phosphatase inhibitors (Roche). Protein samples were quantified with Pierce BCA Protein Assay Kit (23227, ThermoScientific), loaded and separated in pre-cast NuPAGE 10% Bis-Tris Gel (Novex, ThermoScientific) and blotted into PVDF membranes (ThermoScientific). The filters were blocked and incubated with primary and secondary antibodies. Reactive bands were revealed by LiteAbloT EXTEND or LiteAbloT PLUS (Euroclone), and quantified using the ImageJ software.

Primary antibodies used were: mouse anti-Smad4 (1:200; Santa Cruz); mouse anti- β -actin (1:4000; Sigma Aldrich); rabbit anti-P-Smad2 (1:1,000; Cell Signaling); rabbit anti-P-Smad1/5/8 (1:1,000; Millipore); rabbit anti-P-JNK (1:500; Cell Signaling); rabbit anti-P-p38 (1:1,000 Cell Signaling); rabbit anti-P-ERK1/2 (1:500; Santa Cruz); rabbit anti-P-TAK1 (1:500, Cell Signaling); rabbit anti-TAK1 (1:1000, Bethyl); rabbit anti-RelA/p65 (1:1000; Santa Cruz); rabbit anti-P-(S536)RelA/p65 (1:1,000; Cell Signaling). Secondary antibodies (Bethyl) were used 1:1,000.

Gene Expression Analysis

RNA was extracted from the media of the ascending aorta by Trizol (Invitrogen), after removal of adventitia layer. Real-time RT-PCR reactions were run with the Rotor-Gene Q Real time PCR system (QIAGEN). Relative expression amounts were calculated using the $\Delta\Delta$ Ct method with normalization to the concentration of S16 in the same samples. Data are presented as fold changes compared to the control groups. Sequences of specific primers were designed by Primer3 software and are listed in the [Key Resources Table](#).

QUANTIFICATION AND STATISTICAL ANALYSIS

Sample size for all the experiments was pre-estimated from previously published research and from pilot experiments performed in our laboratories. Data are presented as mean \pm SEM. Data distribution was assessed with the Shapiro-Wilk normality test and D'Agostino Pearson test, and assumption of homogeneity of variance was tested using Levene's test for equality of variances. When unequal variance between groups was observed, a Welch correction was performed for all comparisons. Statistical

significance was assessed with the appropriate test according to each experimental design, as detailed in figure legends. After assessing distribution of each data setting, we applied Student's *t* test for independent samples or Mann-Whitney for independent samples, according to the experimental design and as specified in the figure legends. Multiple group analysis was performed with one-way ANOVA or two-way ANOVA followed by Bonferroni's post hoc for data with normal distribution. Analysis for repeated-measures was applied when required by the experimental setting. Multiple group analysis of non-parametric data was performed with Kruskal-Wallis test followed by Dunn's multiple comparison test. $p < 0.05$ was considered significant. Statistical analyses were performed with SPSS 23.0 (IBM Software) and graphs were made with GraphPad Software PRISM5.